Lawrence Berkeley Laboratory
UNIVERSITY OF CALIFORNIA

Materials & Molecular Research Division

To be presented at the TMS/ASM "Treatises in Metallurgy," USA/China Bilateral Metallurgy Conference, Beijing, People's Republic of China, November 1981; and to be published in the Proceedings

THERMODYNAMICS AND KINETICS OF PHASE SEPARATION

D. de Fontaine

June 1981

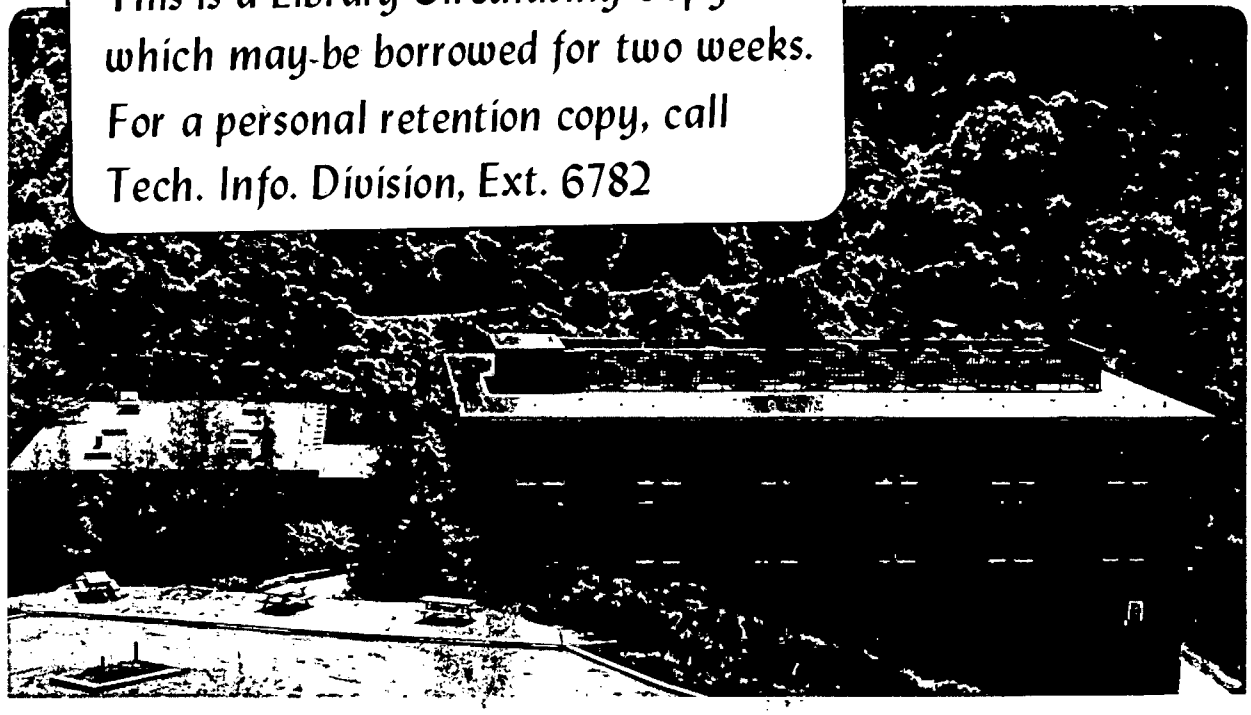

Prepared for the U.S. Department of Energy under Contract W-7405-ENG-48

DISCLAIMER

To be published in TMS/ASM "Treatises in Metallurgy"; USA/China Bilateral Metallurgy Conference; November, 1981; J. Elliot, J. K. Tien, editors.

THERMODYNAMICS AND KINETICS OF PHASE SEPARATION

D. de Fontaine

Lawrence Berkeley Laboratory
Department of Materials Science and Mineral Engineering
University of California
Berkeley, California 94720 USA

1. INTRODUCTION

The art of the Physical Metallurgist is the control of properties through microstructure. Microstructure, in turn, is controlled by bringing about certain phase changes, usually carried out far from thermodynamic equilibrium. Of central practical importance, then, are temperature-time-transformation (TTT) diagrams, of the type shown in Figure 1. Such diagrams determined experimentally, indicate to the alloy designer, after how long (t = time) an isothermal heat treatment (T = temperature) will yield a given new phase β (or mixture of phases) from a parent α phase, stable above the thermodynamic α → β equilibrium temperature T_0. Two T-vs.-log t curves are usually plotted: one (full line) which indicates the "start" of the transformation when, say 1% of α has transformed, and an "end" curve (dashed line) when, say 99% of α has transformed. Considerable use is made of TTT diagrams in the heat treating of steels, for example (1).

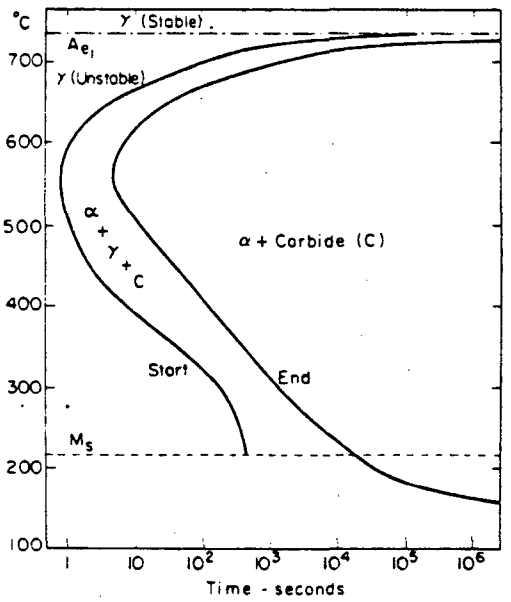

Figure 1. TTT diagram (C-curve) for a plain carbon eutectoid steel.

A typical diagram for an alloy steel is shown in Figure 2. It is seen that the C-shaped curve of Figure 1 has become an S-shaped curve. This feature is thought to be due to the appearance, at lower transformation temperatures, of a variant of the β phase, say β', for which a separate C-curve might exist, and which could be determined experimentally were it not for the interference of the stable product β. The S-curve can then be thought of as resulting from the combination of two or more C-curves. Not only can a C-curve transform to an S-curve on alloying, but the whole "start" curve often shifts laterally to much longer aging times. Slower transformation rates may be beneficial for transformations in steels in order to produce a Martensic product which appears from γ (Austenite) almost instantaneously below a certain temperature, indicated by the horizontal line labeled M_S in Figure 2. Therefore, in order to produce Martensite upon continuous cooling from a temperature in the stable γ range, it is necessary to prevent formation of the normal transformation products (pearlite, bainite), hence to avoid the "nose" of the C-curves. Clearly a shift of the transformation curves to longer times will promote the formation of martensite under far less severe quenching conditions.

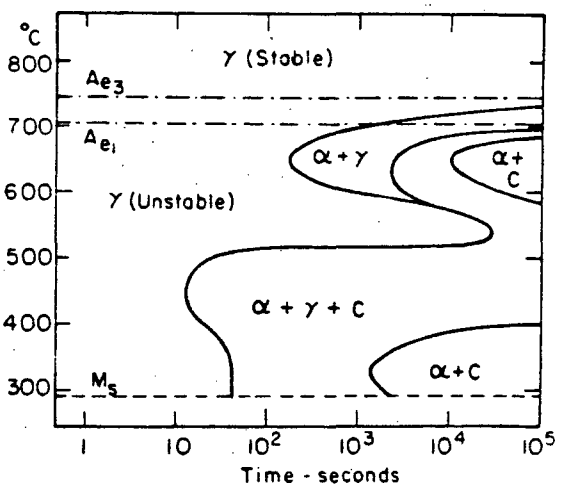

Figure 2. TTT diagram (S-curve) for a 0.33% C, 0.45% Mn, 1.97% Cr steel.

It is quite impossible to predict theoretically the TTT diagram for a given alloy of given composition. At best, one can attempt to understand the mechanisms underlying such basic features as: the transition temperature T_0, the shapes of the individual C-curves, the transformation rates. The most basic concept required is that of nucleation of a new phase or phases (β) from the parent (α). Hence, the major portion of this article will be devoted to nucleation theory, with emphasis placed on the fundamental difficulties encountered in trying to develop a tractable model valid for transformations near and far from equilibrium states. Indeed, even for the simplest of physical situations, homogeneous nucleation

in single-component fluids, the nucleation problem turns out to be one of the most difficult ones encountered in the physical sciences.

There exists a number of excellent reviews or textbooks which cover substantially the same material as presented here in greater or lesser detail; in particular, there is a very thorough treatise of J. W. Christian entitled "The Theory of Transformations in Metals and Alloys" (2). The basics of phase transformations in solids has also been reviewed more succintly by a number of authors, one of the best expositions being that of D. Turnbull (3). Nucleation Theory has been covered, from the metallurgist's viewpoint, in two reviews by K. C. Russell (4, 5). The latter very recent article constitutes an excellent introduction to the extensive work on nucleation in solids by the Aaronson-Lee-Russell school. In that context, the didactic article of H. I. Aaronson (6) should prove to be very valuable to students in this field. Some fundamental aspects of nucleation were covered in a short article by J. W. Cahn (7); spinodal decomposition was covered by the same author (8) and also by J. H. Hilliard (9) and the present author (10). Both topics are treated together in a most lucid and complete manner by Martin (11). This latter article is the text of a course given at the summer school of Aussois (France) in 1978. The courses taught there covered virtually every important aspect of phase transformations in Materials Science, and were recently published (in English) in book form. The reader interested in the more theoretical aspects are referred to the articles by Reiss (12, 13), Langer (14, 15), Binder (16, 17) and their co-workers. Nucleation thermodynamics, to be covered presently, follows the classic texts of Gibbs (18) and of Landau and Lifshitz (19).

2. NUCLEATION THERMODYNAMICS

Because of problems related to anisotropic elastic strain energy and interfacial energy in solids, only fluid phases will be considered here, more specifically, condensed fluids, i.e., multicomponent liquids. At equilibrium, fluctuations in density and/or concentration constantly occur. Occasionally, in a small region, a fluctuation so large may arise that it becomes more stable than the outlying region and actually grows, or matures, at the expense of the latter. In that case, it is said that a supercritical fluctuation has been created, or that a nucleation event has taken place.

Supercritical fluctuations are usually highly improbable and are characterized by large local departures from average concentrations or densities. A schematic representation of a concentration fluctuation in a two-component solution is given in Figure 3a, each vertical bar being located at an atomic position (along one dimension) and representing the concentration distance from pure A or pure B to the average B concentration c^0. For convenience, an averaging procedure, called coarse-graining, is then introduced: the discrete picture of Figure 3a is made continuous by counting up and down bars in a small region of space (coarse grain) so as to define a local average concentration c, plotted as a deviation from the overall average in Figure 3b. The size for these coarse grains over which the average is taken gives rise to some difficulties, as discussed, for example, by Langer (15, 20).

Let us now determine the probability of formation of such a fluctuation in an otherwise uniform system, in the sense of the coarse-graining just introduced. To that effect, let us consider a closed system of finite volume V embedded in a very large reservoir, the latter having constant pressure $\bar{P}$ and temperature $\bar{T}$. The reservoir and system together comprise a very large "universe" assumed to be bounded by perfectly rigid adiabatic walls. Any change occurring in the system gives rise to changes in the extensive variables U, V, S (internal energy, volume, entropy) of the system and of the reservoir ($\bar{U}$, $\bar{V}$, $\bar{S}$). We have

$$\Delta U_{tot} = \Delta U + \Delta \bar{U} = 0$$

$$\Delta V_{tot} = \Delta V + \Delta \bar{V} = 0$$

$$\Delta S_{tot} = \Delta S + \Delta \bar{S} \neq 0$$

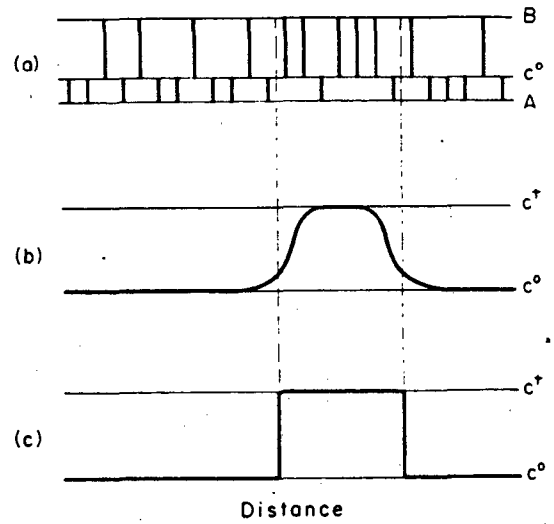

Figure 3. Schematic representations of a (one-dimensional) concentration fluctuation in a binary alloy A-B. (a) atomic distribution about the mean c^0, (b) diffuse interface profile, (c) sharp interface profile.

For the reservoir,

$$\Delta \bar{U} = \bar{T}\Delta \bar{S} - \bar{P}\Delta \bar{V}$$

so that

$$-T\Delta S_{tot} = \Delta U - \bar{T}\Delta S + \bar{P}\Delta V = W ,$$

where W is seen to be the reversible work of formation of the fluctuation.

The probability of formation of an unlikely fluctuation is approximately given by

$$\mathcal{P} = \omega^{\dagger}/\omega^0$$

where $\omega^{\dagger}$ is the number of ways of realizing that type of fluctuation, and ω^0 that of realizing the uniform phase. By the microcanomical formula

$$S = k \ln \omega ,$$

where k is Boltzmann's constant, we have

$$\Delta S_{tot} = S^{\dagger} - S^0 = k \ln \omega^{\dagger}/\omega^0 < 0$$

so that

$$\mathcal{P} = e^{\Delta s_{tot}/k} = e^{-W/kT} . \qquad (1)$$

Since we further assume that, at all times, the temperature T and overall pressure P of the system are equal to those of the reservoir, we shall henceforth drop the bars over T and P. Hence, the work of formation becomes

$$W = \Delta F + P\Delta V , \qquad (2)$$

F being the Helmholtz free energy U - TS.

2.1. Sharp Interface Model

It is now necessary to express W in terms of variables internal to the system; local concentrations (mole fractions), volumes, etc. What is then usually done is to further approximate the fluctuation profile, such as that of Figure 3b, by a simpler one, such as that of Figure 3c, consisting of the outer region (^{0}) of volume V^0 of uniform concentrations c_i^0, and partial molar volumes v_i^0, and an inner region ($\dagger$) of volume $V^\dagger$ of uniform concentrations $c_i^\dagger$ and partial molar volumes $v_i^\dagger$ (i = 1, 2, ... n). Such is the so-called capillarity approximation. The location of the sharp interface separating the fluctuation ($\dagger$) from the homogeneous region (^{0}) must be decided by an appropriate convention; Gibbs (18) chooses that which makes the interfacial energy σ equal to a surface tension defined in the usual mechanical way. With this choice, and for a spherical volume $V^\dagger$, Gibbs further shows that σ is independent of the sphere radius r.

The outer region (^{0}) may be considered as a bulk phase and classical (bulk) thermodynamics may be applied to it. The ($\dagger$) region, however, requires special consideration: although actually of inhomogeneous nature, the fluctuation can find itself in (unstable) equilibrium with the bulk (^{0}), in which case the chemical potentials $\mu_i^\dagger$ are regarded as numerically equal to the corresponding ones μ_i^0 in the bulk (^{0}). The $\mu_i^\dagger$ are then defined operationally as the change in Gibbs free energy (G = F + PV) when a small amount of substance i is added to the $V^\dagger$ region at constant P and T. For a bulk phase, the concentrations c_i do not change in such an operation; but in the present case, since the fluctuation is so small in extent, the $c_i^\dagger$'s cannot be maintained constant. Hence, in general, the $\mu_i^\dagger$ so defined are not those which would be found in a bulk phase of identical average concentrations and pressure.

With these words of caution, we may now proceed. The particularly clear treatment given by Landau and Lifshitz (19) will be followed. In Equation (2), the Δ's have meaning of "final state" (system containing fluctuation $\dagger$) minus "initial state" (system completely homogeneous). Since V^0 is assumed to be so much larger than $V^\dagger$, the transfer of $N^\dagger$ moles (or atoms) of constituents from bulk to fluctuation causes no appreciable change in state (^{0}), so that the bulk phase may be subtracted out of Equation (2). Denoting initial and final states by subscripts $_1$ and $_2$ we have

$$W = F_2 - F_1 + P\Delta V^0 + PV_2^\dagger - PV_1^\dagger + A\sigma ,$$

since the final state (with fluctuation) contains an interface of area A, say, and of (isotropic) surface tension σ. Indeed, because of surface tension, the fluctuation will be under pressure $P^\dagger >> P^0 = P$. Then, after adding and subtracting the term $P^\dagger V_2^\dagger$, we have

$$W = G_2 - G_1 - V^\dagger\Delta P + A\sigma , \qquad (3)$$

where

$$\Delta P = P^\dagger - P^0 , \qquad (4)$$

and where $P\Delta V^0$, a term small compared to W at ordinary pressures, has been discarded. In Equation (3), G_1 stands for the free energy required to extract $N_i^\dagger$ moles (molecules, atoms) of i (i = 1, ... n) from the bulk at T and P:

$$G_1 = \sum_{i=1}^{n} \mu_i^0 N_i^\dagger = N^\dagger \sum_{i=1}^{n} \mu_i^0 c_i^\dagger .$$

Since this expression is linear in $c_i^\dagger$, with coefficients μ_i^0, it represents, by the intercept rule, a point of coordinates $c_i^\dagger$ on the plane tangent at c_i^0 to the Gibbs free energy surface of the homogeneous phase α [see Figure 4 for a binary example]. Since

$$G_2 = N^\dagger \sum_{i=1}^{n} \mu_i^\dagger c_i^\dagger ,$$

where $\mu_i^\dagger$ are the true chemical potentials in the fluctuation region, under pressure $P^\dagger$, we have, under (unstable) equilibrium conditions [$\mu_i^0 = \mu_i^\dagger$]

$$G_1 = G_2$$

and hence, from Equation (3)

$$W = - V^\dagger\Delta P + A\sigma , \qquad (5)$$

an important formula, first given by Gibbs.

The work of formation W can be expressed in a more convenient way by integrating the Gibbs free energy of ($\dagger$) from pressure P^0 to pressure $P^\dagger$:

$$G^\dagger(P^\dagger) = G^\dagger(P^0) + \int_{P^0}^{P^\dagger} V^\dagger(p,T)\, dp \simeq G^\dagger(P^0) + V^\dagger(P^\dagger - P^0) , \qquad (6)$$

the latter equality being obtained by considering the ($\dagger$) material as incompressible. Thus, by Equations (4) and (5)

$$W \simeq V^\dagger\Delta G_v + A\sigma , \qquad (7)$$

where

$$\Delta G_v \simeq - \Delta P$$

is the vertical distance from the tangent plane to $G^0(P)$ at c_i^0 to the free energy surface $G^\dagger$ at the ambiant pressure P^0, at composition $c_i^\dagger$, the Gibbs functions being normalized to unit volume of ($\dagger$). This "tangent construction" is illustrated in Figure 4. A tacit assumption is usually made: that ΔG_v refers entirely to Gibbs free energy surfaces of bulk phases. Actually the derivation of Equation (6) was performed on free energies of non-uniform fluctuation regions so that G^0 may be regarded as corresponding to a point on the G^α free energy surface of bulk α phase (parent phase), which is correct, and $G^\dagger$ may then be regarded as corresponding

to a point on the G^β free energy surface of bulk nucleating phase, at $P^\dagger$ and T, which is not strictly correct. This may lead to some confusion, or to alternate definitions of chemical potentials, as will presently be shown. In both Equations (5) and (7) the first term in the work of nucleation is negative and represents the driving force for nucleation. The second term represents the positive work of forming the interface.

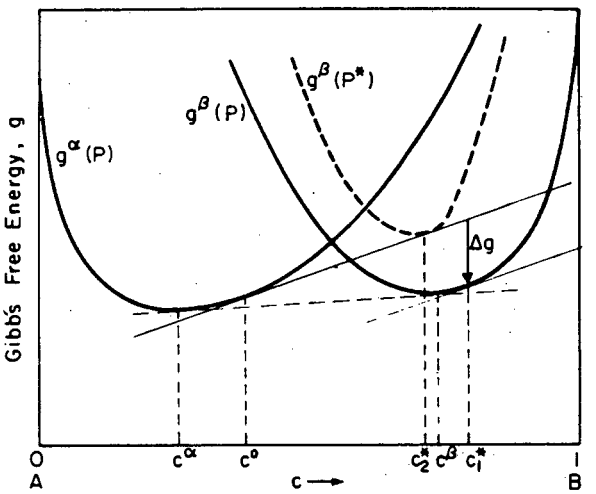

Figure 4. Gibbs free energy curves for a binary fluid. Concentration c_1^* is that obtained by maximizing the quantity Δg (tangent construction), c_2^* might be the concentration of the critical nucleus if the concentration dependence of the interface were taken into account.

The internal variables characterizing the fluctuation in equilibrium must now be determined. For this purpose, the fluctuation volume $V^\dagger$ will be assumed spherical of radius r. We may then take r and n - 1 independent concentration variables as the internal variables of W and express the condition of equilibrium thus:

$$\left(\frac{dW}{dr}\right)_{P,T,c_i} = 0$$

$$\left(\frac{dW}{dc_i}\right)_{P,T,r,c_{j\neq i}} = 0 \quad (i = 1, 2, \ldots n-1).$$

The first condition yields

$$\Delta G_v \frac{\partial V}{\partial r} + \sigma \frac{\partial A}{\partial r} = 0 , \qquad (8)$$

since the free energies at constant T, P, $c_1 \ldots c_n$ are invariant, and since σ is independent of radius of curvature. Equation (8) yields the critical radius r^*:

$$r^* = \frac{2\sigma}{\Delta P^*} \simeq -\frac{2\sigma}{\Delta G_v^*} . \qquad (9)$$

Spherically symmetric fluctuations with $r < r^*$ should decay, those with $r > r^*$ should spontaneously grow.

The denominators ΔP^* or ΔG_v^* are determined by the second condition. If the interfacial energy σ is independent of concentration, this condition requires the vertical distance between the G^0 tangent hyperplane and the G^β surface to be a maximum. The critical composition c_i^* (i = 1, ... n) is thus obtained by constructing another tangent plane to the lowest portion of the G^β surface parallel to that at c_i^0 to G^α. This is shown for a binary example in Figure 4. This approximation is fairly reliable if the degree of supersaturation (or of undercooling) is small, i.e., if ΔG_v is small in magnitude.

If supersaturations are large, and particularly if the coarse-grained free energy of a condensed-phase solution is given by a continuous smooth curve such as that of Figure 5, then σ can no longer be considered as composition-independent. In that case, the search for equilibrium is best carried out, following Reiss and Shugard (R-S, 13), by taking derivatives of W with respect to an alternate set of independent variables, the fractional number of moles $N_1, N_2 \ldots N_n$:

$$\left(\frac{dW}{dN_i}\right)_{P,T,N_{j\neq i}} = 0 .$$

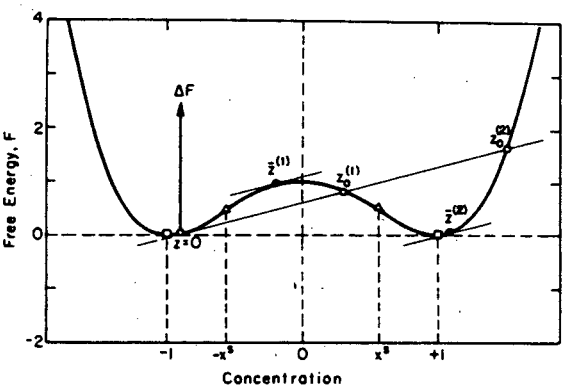

Figure 5. Continuous (coarse-grained) free energy curve for use in coherent nucleation. Curve is plot of Equation (49).

One then readily obtains the equilibrium condition (13)

$$\mu_i^\beta + (P^\beta - P)V_i^\beta + A\sigma_i = \mu_i^\alpha , \qquad (10)$$

the subscripts on V and σ indicating derivatives with respect to $N_i^\dagger$. In this equation μ_i^β is the chemical potential of i in bulk β at pressure P^0. The first two terms together yield $\mu_i^\beta(P^\beta)$, the chemical potential of i in bulk β at the pressure of the critical fluctuation, or critical nucleus. Surprisingly, the condition of equality of chemical potentials no longer holds here because of the presence of the correction term $A\sigma_i$. Thus, as announced, this derivation has led to an alternate definition of chemical potentials ($\mu_i^\beta \neq \mu_i^\dagger$), which is, however, a useful one, as it allows the concentration of the critical nucleus to be determined in cases of large supersaturations. Indeed, R-S (13) show that, as c_i^0 tends to the so-called spinodal concentrations c_i^s, at which the second derivatives of G with respect to concentration vanish, $c_i^\dagger$ correspondingly moves inward towards the same spinodal composition. The same conclusion can be reached by adopting quite a dif-

ferent model for the critical nucleus, as proposed by Cahn and Hilliard (C-H, 21, 22). This model will be examined later (Section 2.2).

The work of formation of the critical nucleus can be obtained by substituting for r^*, from Equation (9) into Equations (5) or (7):

$$W^* = \frac{16}{3}\pi\frac{\sigma^3}{(\Delta P^*)^2} = \frac{16}{3}\pi\frac{\sigma^3}{(\Delta G_v^*)^2} . \qquad (11)$$

It is seen that, as the concentration of the α supersaturated phase reaches the equilibrium one given by the common tangent construction, the critical radius r^* and the critical work W^* both tend to infinity as ΔP^* ΔG_v^* both go to zero.

At this point, it is already possible to gain some qualitative insight into some of the features of the TTT diagram of Figure 1. Firstly, the temperature T_0 there indicated is obviously the thermodynamic equilibrium temperature at which ΔG_v vanishes, i.e., for which we have $\mu_i^\beta(P^0) = \mu_i^\alpha(P^0)$. Above T_0, the α phase must be stable toward any β-type fluctuations, of arbitrary magnitude. Below T_0, α should decompose at least partially to β, according to equilibrium thermodynamics. The kinetics of the appearance of transformation products may be very slow, however. In particular, for low undercoolings, W^* is extremely large so that, by Equation (1), the probability of finding a critical fluctuation, which will initiate the transformation, will become vanishingly small. Thus, just below T_0, we expect very long transformation times, as observed (Figure 1). At the other extreme, as T tends to zero absolute, W^*/kT will tend to infinity, again lengthening the transformation times immeasurably. At some intermediate temperature, a shortest transformation time is expected. A more quantitative description of the C-curve must be deferred, however, until a kinetic treatment is given (Section 3).

2.2. Diffuse Interface Model

One may decide not to make the Gibbs construction of "squaring the profile" in Figure 3; then, since a sharp interface term Aσ may no longer be included in the work W, it is necessary to take the fluctuation inhomogeneity into account in another way. This is done formally by allowing each volume element dv to possess a local free energy f(c) dv, where f is a Helmholtz free energy per unit volume evaluated in bulk material having composition c equal to the average composition c(x) in volume dv about point $\underset{\sim}{x}$ [In this section, we shall consider binary solutions only, for simplicity, so that there will be but one independent concentration variable, c, defined to be that of the minority component in the solution]. Such is not, however, the only contribution to the volume element's free energy; no matter how small dv be taken (in the continuum approximation) its composition can never, in general, be regarded as homogeneous. To take this non-uniformity into account, one must assume that the local free energy contains terms depending on the composition gradient (21, 22, 19). Cahn and Hilliard show that the first correction to the local free energy is proportional to the gradient of concentration squared $(\nabla c)^2$. This is because, by symmetry, the gradient correction can only depend on the square of the nabla operator ∇, the other ∇^2, the Laplacian, being then incorporated into the square gradient. In this model, then, the free energy of an arbitrary volume V of a binary solution is expressed as a sum of elementary contributions, thus (21)

$$F = \int_V [f(c) + \kappa(\nabla c)^2]\, dv \qquad (12)$$

where κ is the so-called gradient energy coefficient, assumed to be approximately composition-independent.

To apply Equation (12) conveniently to the nucleation problem, one must assume that the free energy f(c) varies smoothly with c, as shown in Figure 5. Then the "bulk" free energy f(c) is well-defined everywhere at given temperature T and pressure P. The critical nucleus is now that spherically symmetric fluctuation which makes the functional F stationary for all small changes $\delta c(\underset{\sim}{x})$ of the composition profile which leave to average concentration c^0 invariant:

$$\int_V (c - c^0)\, dv = 0 .$$

This auxiliary condition introduces a Lagrange multiplier λ, so that the Euler equation for this variational problem is

$$\frac{\partial L}{\partial c} - \nabla\cdot\frac{\partial L}{\partial \nabla c} = 0 \qquad (13)$$

where the Lagrangian is

$$L(c,\nabla c;\underset{\sim}{x}) = f(c) + \kappa(\nabla c)^2 - \lambda(c - c^0) . \qquad (14)$$

There results the differential equation

$$2\kappa\nabla^2 c = f'(c) - \lambda , \qquad (15)$$

where the accent denotes differentiation with respect to c.

Let us place the origin of a spherical polar coordinate system at the center of the nucleus. Far away from the nucleus, the concentration must be very nearly c^0, and all gradients must vanish. Then, by Equation (15), the multiplier λ must be equal to f_0', the slope of the tangent to f(c) at $c = c^0$. The differential equation (15) then becomes, explicitly,

$$2\kappa\frac{d^2c}{dr^2} + 4\frac{\kappa}{r}\frac{dc}{dr} = f'(c) - f_0' \qquad (16)$$

This second-order ordinary differential equation is nonlinear in the profile function c(r) because of the presence of the derivative f'(c). Since the free energy curve, in order to have the features apparent in Figure 5, must be Taylor-expanded at least to fourth order in c, f'(c) must be at least a polynomial of degree three in c. Hence, the critical nucleus profile $c^*(r)$ must be obtained by numerical integration of Equation (16).

The critical work of nucleation W^* is obtained by inserting the (unstable) equilibrium profile c^* into Equation (12) and integrating, after subtracting off the free energy of the uniform solution c^0:

$$W^* \equiv \Delta F = 4\pi\int_0^\infty [\Delta f(c^*) + \kappa\left(\frac{dc}{dx}\right)^2]\, r^2\, dr \qquad (17)$$

where

$$\Delta f(c^*) = f(c^*) - f(c^0) - (c^* - c^0)f_0' \qquad (18)$$

It is seen thatthe latter expression, in different notation, is just the vertical distance from the tangent (at c^0) to the free energy curve at c^*, as in the

classical treatment of the previous section.

Cahn and Hilliard (22) obtained numerical solutions for average concentrations c^0 just inside the phase boundary c^α (common tangent rule), just above the spinodal [c^s, solution of $f''(c) = 0$], and at two concentrations intermediate between these two. These authors concluded that the concentration at the center of the nucleus was such as to make the driving force $\Delta f(c)$ negative, as expected on "classical" grounds. Also, for c^0 just below but close to c^α, the nucleus resembled the classical one with composition at the nucleus center close to c^β, and the nucleus radius becoming very large, along with the work of nucleation W^*. Also, the interface portion of the profile (high gradient) tended to be relatively narrow, with interfacial energy close to that given theoretically for a flat interface. When c^0 was made to move away from c^α, the critical radius at first decreased along with the work of nucleation, as in the classical case. However, unlike the classical model, the concentration at the center of the nucleus tended to decrease towards the average c^0 and the interface became increasingly diffuse. Finally, for c^0 close to the spinodal c^s, the critical radius r^* again became unbounded whilst the work of nucleation continued to drop, becoming zero for c^0 at c^s. In a sense, then, the critical nucleus at the spinodal is the whole uniform solution itself, which therefore now finds itself inherently unstable.

These results are of central importance for the theory of homogeneous nucleation, i.e., in cases where the nucleating phase (β) may be regarded as having the same coarse-grained free energy function as the parent phase (α). In turn, this implies that α and β have basically the same crystal structure, or both be fluids of similar nature. Or, to put it yet differently, the difference between the bulk (^{0}) and the nucleus (†) must be such as to be described entirely by the change in value of a small number of continuously varying "order parameters" ξ_i, in the present case of a binary solution, the unique concentration difference $\xi = c^\dagger - c^0$.

Unfortunately, the difficulty encountered in solving the differential equation (16) has thus far inhibited the application of the Cahn and Hilliard theory to practical cases. There exists, however, a simplified treatment which is, in some sense, intermediate between the full diffuse interface treatment and the classical one. The idea is based upon the Rayleigh-Ritz method of minimizing a functional by parametrizing the unknown function. The integration is then performed on the trial function containing a few judiciously chosen parameters, and the resulting integral is minimized with respect to those parameters. Such a procedure was adopted by this author (23) who chose a standard sharp interface spherical profile, convoluted by a Gaussian curve in order to produce a diffuse interface for which gradients could be evaluated according to the C-H recipe. Two parameters were used: the order parameter ξ (defined above, also called concentration amplitude in the previous work) and an average radius r. The two parameters scaled the profile in any way desired. With this simplified treatment, the main conclusions of the original C-H treatment could be recovered with no great computational effort. It was also concluded, by examining the complete $W(\xi,r)$ surface for various values of c^0 (at constant T), that the singularity of r^* at the spinodal could have but very mild consequences and that there could be no real discontinuity of mechanism at the spinodal, as far as decomposition kinetics were concerned. These conclusions have been well substantiated by more recent work of Langer (20, 24), Binder (16), Lebowitz (25) and coworkers. We shall return to this question in Section 3.4.

One may also consider classical nucleation as a highly simplified Rayleigh-Ritz treatment of C-H formulation. This is done by performing the integration (17) in three portions

$$W^* = 4\pi \left\{ \int_0^{r^*} + \int_{r^*}^{r^*+\delta r} + \int_{r^*+\delta r}^{\infty} \right\} .$$

The first and third integrals are performed over regions of roughly uniform compositions, so that the gradients are taken to be zero. The first integral then yields, by the mean value theorem,

$$4\pi\, \Delta f(c^\dagger) \int_0^{r^*} r^2\, dr = \frac{4}{3}\pi\, r^{*2}\, \Delta f ,$$

whilst the third integral vanishes along with $\Delta f(c^0)$. The second integral is over a spherical shell of thickness δr and is naturally identified with the interfacial free energy $A\sigma$, in the present case, $4\pi r^{*2}\sigma$. If σ is assumed to be concentration-dependent (as calculated, say, by the C-H formula), one recovers the treatment of R-S (13). If σ is considered to be concentration-independent, one recovers the standard classical treatment but then, conclusions regarding the behaviour of r^* and W^* near the spinodal are irrevocably lost.

3. NUCLEATION KINETICS

Although we now know from Equation (1) that the probability of finding an embryo located on any one of the N lattice sites of a crystal will be

$$\mathcal{P} = Ne^{-W/kT} , \qquad (19)$$

still, we have as yet little information about the actual rate of formation of nuclei, i.e., about nucleation kinetics *per se*. Such information can be obtained in an approximate manner by treating the problem in a way first suggested by Farkas (26), Volmer and Weber (27), Becker and Döring (28). The original idea was extended by Reiss to the problem of binary solutions (12). We shall treat here directly the multicomponent case, in a simplified version of the more complete (and more correct) treatment of Langer (14, 15) and of B-S (16).

3.1. Cluster Diffusion Equation

We begin by considering that the growth of a cluster of atoms, or embryo, or protonucleus, takes place by chance collisions with smaller ones. Likewise, decay is caused by a cluster's splitting up into smaller subunits. Clusters are considered to be essentially unlocalized and non-interacting. Although B-S (16), for example, allow the addition or removal of arbitrary subunits to a given cluster, and even the coagulation of a pair of clusters to form a larger entity, we shall follow the usual practice of allowing growth or decay by the addition or removal of single atoms (or molecules, or monomers) only to the embryos. Graphically, a cluster can be thought of as moving by discrete nearest-neighbor jumps in an n-component lattice (n = number of molecular species), as indicated schematically (for n = 3) in Figure 6.

At given time t, let the concentration of cluster characterized by coordinates $N_1, N_2 \ldots N_n$ be $C(N_1, N_2 \ldots N_n;t)$ or $C(\underline{N})$ for short, where, as above, N_i denote number of atoms (or molecules) of type i. Of course, it is assumed that the embryos all have some standard simple shape, such as the spherical one. Additional variables could be included to take care of changes of shape, but this will not be done here.

The time rate of change of embryo concentration may be written formally as

$$\frac{\partial C(\underset{\sim}{N})}{\partial t} = -\sum_{j=-n}^{n}{}' J_j(\underset{\sim}{N}) \ , \qquad (20)$$

where the summation is over all positive and negative directions in multicomponent space (j ≠ 0 excluded). Hence, this summation represents the discrete-space divergence of the flux vector in direction j:

$$J_j(\underset{\sim}{N}) = -[\beta_{N_j} C(\underset{\sim}{N}) - \alpha_{N_j+1} C(\{N_j + 1\})]. \qquad (21)$$

In this equation, β_{N_j} is the intrinsic rate of attachment of atoms of type j to a cluster containing $N_1 \ldots N_n$ atoms, whilst α_{N_j+1} is the intrinsic rate of loss of atoms of type j from a cluster containing $\{N_j + 1\} \equiv N_1, N_2, \ldots, N_j + 1, \ldots N_n$ atoms. Both α and β are positive quantities. Thus, Equations (20) and (21) merely indicate that the rate of change of concentration of clusters at $\underset{\sim}{N}$ is made up of single nearest-neighbor steps to $\underset{\sim}{N}$ from neighboring sites on the n-dimensional lattice of embryos (Figure 6), or away from $\underset{\sim}{N}$ to nearest neighbor sites.

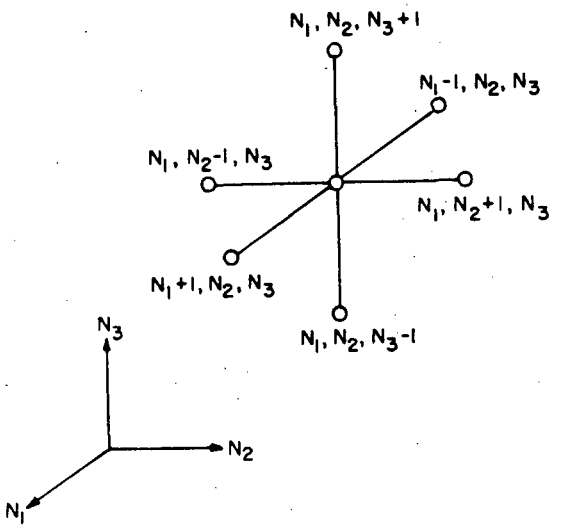

Figure 6. "Lattice" of embryos for a three-component system. Jumps are from center ($\underset{\sim}{N}$) to (or from) nearest neighbor sites.

Let us now consider the equilibrium distribution of clusters for which all fluxes J_j vanish identically everywhere. Then, if we restrict consideration to those clusters small enough so that their work of formation W is positive, we shall have at equilibrium, by Equation (19), the Boltzmann-like distribution

$$C^0(\underset{\sim}{N}) = N\, e^{-W(\underset{\sim}{N})/kT} \qquad (22)$$

Then,

$$J_j^0(\underset{\sim}{N}) = 0 = -\beta_{N_j} C^0(\underset{\sim}{N}) + \alpha_{N_j+1} C^0(\{N_j + 1\}) \qquad (23)$$

and therefore

$$\alpha_{N_j+1} = \beta_{N_j} C^0(\underset{\sim}{N})/C^0(\{N_j+1\}) \ . \qquad (23)$$

We now make the daring assumption (detailed balancing) that the relation (23) for the evaporation rate α is valid even for non-equilibrium situations. By eliminating α from Equations (20) and (21) by means of (23) we then find:

$$\frac{\partial C(\underset{\sim}{N})}{\partial t} = -\sum_{j=1}^{n} \left[\beta_{N_j} C^0(\underset{\sim}{N}) \left(\frac{C(\underset{\sim}{N})}{C^0(\underset{\sim}{N})} - \frac{C(\{N_j + 1\})}{C^0(\{N_j + 1\})}\right)\right.$$

$$\left. + \beta_{N_j - 1} C^0(\{N_j - 1\}) \left(\frac{C(\underset{\sim}{N})}{C^0(\underset{\sim}{N})} - \frac{C(\{N_j - 1\})}{C^0(\{N_j - 1\})}\right)\right] .$$

For N_j sufficiently large, differences may be replaced by derivatives to yield the continuity equation

$$\frac{\partial C}{\partial t} = -\sum_{j=1}^{n} \frac{\partial J_j}{\partial N_j} \ , \qquad (24)$$

with flux given by

$$J_j = -\beta_j C^0 \frac{\partial (C/C^0)}{\partial N_j} \ , \qquad (25)$$

where the explicit N-dependence has been left out for simplicity. Equation (25) indicates that the embryo flux is proportional to the gradient of a concentration ratio times a positive mobility β_j. This is clearly seen when Equation (25) for the components of the flux vector $\underset{\sim}{J}$ are written in matrix notation:

$$\underset{\sim}{J} = -\underset{\approx}{B}\underset{\sim}{X} \ ; \qquad (26)$$

here $\underset{\sim}{X}$ is a generalized force vector and $\underset{\approx}{B}$ is an n×n mobility matrix. In Equation (26), B is diagonal, but it need not be. Indeed, in Binder's (16) or Langer's (14) analyses, where growth or decay of clusters can be accomplished by more general mechanisms than the monomer addition (or deletion) considered here, the mobility matrix is non-diagonal. The same is true for Russell's (29) "linked-flux" mechanism. In general, then, the $\underset{\approx}{B}$ matrix need be merely symmetric (by the Onsager reciprocity relations) and positive definite (by the Second Law):

3.2. Solution of Kinetic Equation

Equations (24) and (25) may be combined to yield a diffusion equation for the cluster concentration $C(\underset{\sim}{N},t)$:

$$\frac{\partial C}{\partial t} = \sum_{i=1}^{n} \frac{\partial}{\partial N_i} \left[\beta_{ij} C^0 \frac{\partial (C/C^0)}{\partial N_j}\right] \qquad (27)$$

In Equation (27), off-diagonal mobility elements have been included for generality. This linear equation is first-order in time t and second-order in "space" $N_1, \ldots N_n$, the space itself being anisotropic because of "skewing"

due to the mobility matrix. Also, space is inhomogeneous since the coefficients of the $\partial/\partial N_j$ differentials depend on position through C^0, i.e., through the work $W(\underline{N})$. Thus, for n > 1, even for steady-state, the diffusion equation can only be solved numerically. Note that Equation (27) can also be written in the form of a Fokker-Planck equation

$$\frac{\partial C}{\partial t} = \sum_{i,j=1}^{n} \left[\beta_{ij} \frac{\partial^2 C}{\partial N_i \partial N_j} + \beta_{ij} \frac{\partial}{\partial N_i}\left(C \frac{\partial W}{\partial N_j}\right)\right] , \qquad (28)$$

where the N-dependence of β has been neglected for the purpose of the qualitative discussion which follows.

The physical situation represented by the differential equation (27) or (28) may be visualized with the help of Figure 7 which depicts schematically a two-dimensional case: an ample supply of monomers, (components 1, 2) is injected at the origin of the N_1,N_2 coordinate system. Since the concentration of monomers at the origin is high, clusters will move away, their growth (i.e., movement towards larger N_i-values) being driven by the cluster concentration gradient represented by the first term in Equation (28). The second term, whose effect is due to a force proportional to the gradient of the W-surface, opposes this motion. Nevertheless, after some incubation time, the first embryos will appear at the top of the saddle point or pass in the energy surface W whose contours are plotted schematically in Figure 7. From the critical nucleus position (*) onwards, it's downhill all the way, and ever-growing nuclei will tumble down into the W = 0 level pool below (indicated by cross-hatching). Ripe clusters are then skimmed off at large-N_i points opposite the origin, along the edge of the shallow pool (dark lines). The boundary conditions are thus: constant unit concentration of monomers close to the origin, and, at the other extreme, zero concentration of large clusters at the pool edge, a completely absorbing boundary. All other boundaries are reflecting (shaded, Figure 7).

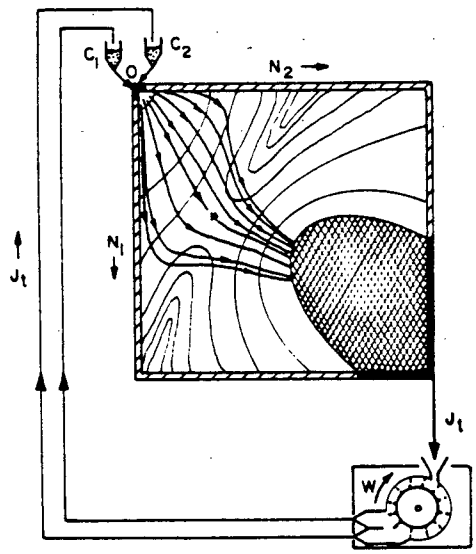

Figure 7. Schematic of steady-state nucleation for a binary system. Contour lines are those of surface $W(N_1,N_2)$, lines with arrow are flow paths of embryos. Shredder-sorter at bottom breaks up mature nuclei into individual monomers and pumps these back up to the holding silos at the origin.

After having been drained off, the large clusters are broken up into constituent monomers in the shredder-sorter indicated below the pool, and pumped back up to the holding silos at the origin. After some time, a steady-state condition will result, with

$$\nabla \cdot J = 0 \qquad (29)$$

for all points in N-space, the total flux being fixed by the boundary conditions, by the height W* of the saddle point, and, to a lesser extent, by the shape of the W-surface itself, in particular, by the magnitude of the principal curvatures of W at the saddle point. The integrated steady-state nucleus flux J* at the pass is the important quantity to calculate. The work of operating the pump must be equivalent to the work of nucleation W*, the energy surface with its saddle point providing the impedence to total matter flow J_t. If the outside flow is interrupted by closing off all inlets and outlets, an equilibrium condition will eventually result, characterized by

$$J_j = 0 \qquad \text{(all j, all } \underline{N}\text{)} ,$$

everywhere. The concentration $C(\underline{N},t)$ for all $\underline{N}$ and all times will thus be $C^0(\underline{N})$, given by Equation (22).

The start curve in TTT diagrams should be determined theoretically as the locus in temperature-time space at which an appreciable nucleation flux over the pass is first observed. Thus, the full time-dependent differential equation should be solved. In practice, the simpler procedure is adopted of locating the start curve by the inverse of the nucleation rate, i.e., of the steady state flux J* (see Section 4.1).

Even the calculation of J* is no simple matter. Langer (14) and Binder (16) give rather elaborate treatments of saddle-point flux determination in n-component systems. To simplify matters, we shall here adopt the more transparent, though not quite correct procedure used by Reiss (12) for binary systems. The trouble with the latter treatment is that it assumes that the vector J* at N_i* is along the direction of maximum negative curvature at the saddle point. Unfortunately, this is not justified, as the influence of the mobility matrix $\underline{B}$ is such that, in general, cluster flux will be biased in the direction of the fastest moving monomer. Actually, then, one should first render the space isotropic by a suitable coordinate transformation, as done, for instance, by Russell (29) in a special case; then J* can be taken as parallel to the line of steepest descent of W* in the new coordinate system. Unfortunately, by so doing, one buries the elements of the mobility matrix inside the coordinate transformation, so that such important parameters as intrinsic diffusivities disappear inside certain eigenvalues with which the final answer is expressed. For this reason, we shall be content here to generalize the Reiss treatment to n-component systems, keeping in mind that this approximation will tend to work best in such situations where the skewing affect of unequal mobilities is not too great, and nuclei grow from monomers at constant concentration.

At the saddle point, the W-surface may be expanded to second order

$$W^* \equiv W(\underline{N}^*) = W_0^* + \tfrac{1}{2} \sum_{i,j=1}^{n} \left(\frac{\partial^2 W}{\partial N_i \partial N_j}\right)_{\underline{N}^*} \delta N_i \delta N_j \qquad (30)$$

where

$$\delta N_i = N_i - N_i^* \qquad (i = 1, \ldots n) .$$

The linear term in the expansion vanishes because W has a horizontal tangent plane at $\underset{\sim}{N}^*$. Since the second-derivative matrix ($\underset{\sim}{W}''$, say) is symmetric, it is diagonalized by a uniquely-defined real orthogonal matrix R whose column vectors are the eigenvectors of W, pointing along the principal curvature directions. The eigenvalues λ_i (i = 1, ... n) of $\underset{\sim}{W}''$ measure the curvatures themselves. The nature of the problem at hand dictates that there shall be one negative eigenvalue, say λ_1, all others being positive. By Equation (30), the W-surface at the saddle point may now be approximated by

$$W^* = W_0^* + \tfrac{1}{2} \sum_{i=1}^{n} \lambda_i \, \delta\bar{N}_i^2 \, , \tag{31}$$

where the over-line denotes, here and below, variables having been transformed by the change in coordinate system brought about by the rotation operator R.

Define transformed fluxes and forces, according to the matrix notation of Equation (26), by

$$\underset{\sim}{\bar{J}} = \underset{\sim}{R}\underset{\sim}{J} \, ,$$

$$\underset{\sim}{\bar{X}} = \underset{\sim}{R}\underset{\sim}{X} \, .$$

The transformed flux equation reads

$$\underset{\sim}{\bar{J}} = \underset{\sim}{A}\underset{\sim}{\bar{X}} \tag{32}$$

where

$$\underset{\sim}{A} = \underset{\sim}{R}^{\dagger}\underset{\sim}{B}\underset{\sim}{R} \, , \tag{33}$$

the dagger denoting the operation of transposition. The force components X_i (i = 1, ... n) can be recovered from Equation (32) by inversion

$$\underset{\sim}{\bar{X}} = \underset{\sim}{A}^{-1}\underset{\sim}{\bar{J}} \, . \tag{34}$$

We now make the simplifying assumption, discussed above, that the flux vector in the rotated coordinate system $\bar{N}$ is along the line of largest negative curvature of W*, i.e., that all the flux at the saddle point is over and down the steepest slope of W*. Therefore, by assumption we have,

$$\underset{\sim}{\bar{J}}^{\dagger} = (J_1^*, \, 0, \, \ldots, \, 0).$$

Consequently, we have, by Equation (34), the very simple result

$$J_1^* = a_{11}^{-1} \, \bar{X}_1 \tag{35}$$

where a_{11} is the first element of the inverse of the $\underset{\sim}{A}$ matrix. Expressions for a_{11} will be given in Section 3.3.

The problem of finding the steady-state flux has thus been reduced to an essentially one-dimensional one, to which the standard method of solution of Frenckel (30) applies. Equation (35) becomes, explicitly

$$J_1^* = -M^* \, C^0 \left(\frac{d(C/C^0)}{d\bar{N}_1} \right)_{\bar{N}_{i \neq 1}} \, , \tag{36}$$

where M*, an effective mobility, denotes the value of a_{11}^{-1} at the saddle point. The integration of Equation (36) will be carried out in the vicinity of $\bar{N}^*$, along $\bar{N}_1$ only, at constant M*. We have, according to the boundary conditions specified earlier,

$$J_1^* \int_1^{\infty} \frac{d\bar{N}_1}{C^0} = M^* \int_1^{0} d(C/C^0) = M^* .$$

By using expression (22) for the equilibrium concentration C^0, and by making use of the quadratic expansion (31) for W* we have

$$\int_1^{\infty} \frac{d\bar{N}_1}{C^0} \simeq \frac{1}{N} \, e^{(W_0^* + \frac{1}{2} \sum_{i=2}^{n} \lambda_i \, \delta\bar{N}_i^2)/kT}$$

$$\times \int_{-\infty}^{\infty} e^{-|\lambda_1| \, \delta\bar{N}_1^2/2kT} \, d\delta\bar{N}_1$$

so that

$$J_1^* = NM^* \left(\frac{|\lambda_1|}{2\pi kT} \right)^{\frac{1}{2}} e^{-(W_0^* + \frac{1}{2} \sum_{i=2}^{n} \lambda_i \, \delta\bar{N}_i^2)/kT} .$$

The total flux J* over the pass may now be obtained by integrating J_1^* over the remaining variables ($\bar{N}_2$, ..., $\bar{N}_n$) in the immediate vicinity of the saddle point to obtain:

$$J^* = K \, e^{-W_0^*/kT} \tag{37}$$

where the kinetic prefactor K is given by

$$K = NM^*ZY \, , \tag{38}$$

Z being the Zeldovich factor

$$Z = \left(\frac{|\lambda_1|}{2\pi kT} \right)^{\frac{1}{2}} \tag{39}$$

and Y being given by an inverse product of the other (positive) eigenvalues:

$$Y = \prod_{i=2}^{n} \left(\frac{2\pi kT}{\lambda_i} \right)^{\frac{1}{2}} \, . \tag{40}$$

It is remarkable that the kinetic treatment yields a nucleation rate J* proportional to exp(-W*/kT), just as was predicted by the thermodynamic theory. Of course, now some new information has been gained: an explicit albeit approximate, expression for the kinetic prefactor K. As noted by Reiss (12), for given M* (given mobilities β^*_{ij}), K is larger for larger value of the negative curvature $|\lambda_1|$ (steep rise to, and descent from the pass) and smaller for larger positive curvatures (λ_2, ..., λ_n; narrow pass, constricted flux).

3.3. Mobility

For applications to TTT diagrams, we are particularly interested in the temperature dependence of the integrated steady-state flux J*. Equation (37) exhibits a strong T-dependence in the exponential factor, and a much weaker dependence in the Z and Y factors, which we shall disregard. There are, however, other strong exponential temperature dependencies hidden in the effective mobility M*. The simplified diagonalization procedure used in the previous section, coupled with the assumption of a diagonal mobility matrix $\underline{B}$ enables us to write down immediately an explicit expression for M* which, as explained above, is given by the reciprocal of the first element of the matrix

$$\underline{A}^{-1} = \underline{R}^{\dagger}\underline{B}^{-1}\underline{R} ,$$

where $\underline{R}$ is an orthogonal matrix (of elements r_{ij}) and $\underline{B}^{-1}$ is a diagonal matrix of elements $1/\beta_i^*$. Hence, under these assumptions, the effective mobility for an n-component system is given very simply by

$$M^* = \left(\sum_{j=1}^{n} \frac{r_{j1}^2}{\beta_j^*}\right)^{-1} = \frac{\beta_1^*\beta_2^* \ldots \beta_n^*}{\beta_1' r_{11}^2 + \beta_2' r_{21}^2 + \ldots + \beta_n' r_{n1}^2} , \quad (41)$$

where β_j' denotes a product of all n β's divided by the jth one.

There remains the difficult problem of finding suitable expressions for the mobilities β_i^* in a multicomponent solid. It is usually assumed (31) that the mobility of i is proportional to the rate at which i-type monomers (atoms, molecules) strike unit area of the nucleus interface. Random walk theory then allows one to write β_i^* as proportional to the cluster surface area S, to the concentration (availability) of i monomers in the vicinity of the cluster, and to an atomic jump rate, itself proportional to a suitable diffusivity $\bar{D}_i$, divided by a mean jump distance. Retaining only those terms which will matter in temperature-dependence considerations, we then have:

$$\beta_i^* \sim \bar{c}_i \bar{D}_i \quad (42)$$

It is not clear, however, what concentration the $\bar{c}_i$ must represent, nor precisely what $\bar{D}_i$ means physically. Clearly, at least two important mechanisms must play a role: the diffusion of species in the matrix in order to feed the growing nucleus, and the rate at which atoms can successfully cross the matrix-nucleus interface. The problem of matrix diffusion is completely untractable in the present context: as the nucleus grows and migrates, the matrix concentration changes locally; strictly speaking, then, the W energy function itself must constantly change in a very complicated way. Generally, all these subtelties are ignored; but then how is one to take into account the fact that a solute which does not partition (i.e., such that its concentration in both matrix (c_i^0) and nucleus ($c_i^{\dagger}$) is the same) should hardly contribute to the overall mobility? An interesting attempt was made by Russell (29) to take such effects into account: the two basic mechanisms referred to above were considered in an approximate manner by postulating the existence of a "shell" of material intermediate between the matrix proper and the nucleus surface. Then two separate rates were defined: that for transfer of atoms from matrix to shell (β^0) and that for transfer of atoms from shell to nucleus ($\beta^{\dagger}$). The nucleus was assumed to grow at constant composition, this situation defining the classical limit, as will be explained in the next section. The resulting flux equations turned out to be non-diagonal even in the binary solution case considered by Russell. After performing an appropriate canonical (diagonalizing) transformation, Russell obtained the saddle point flux as

$$J^* = NZ \frac{\beta^0\beta^{\dagger}}{\delta^2\beta^{\dagger} + \beta^0} e^{-W^*/kT} , \quad (43)$$

where the correction term

$$\delta = 1 - \frac{c^0}{c^{\dagger}}$$

took into account the fact that a non-partitioning (δ = 0) solute does not contribute to matrix diffusion.

We shall adopt here Russell's result for an effective mobility β_i^* by simply lifting Equation (43) out of context and writing, by analogy, for multicomponent systems,

$$\beta_i^* = \frac{\beta_i^0\beta_i^{\dagger}}{\gamma_i\beta_i^{\dagger} + \beta_i^0} \quad (44)$$

where γ_i is a partitioning correction factor, much like Russell's δ^2, for instance

$$\gamma_i = 2\left|\frac{c_i - c_i^0}{c_i + c_i^0}\right| . \quad (45)$$

Here and below, the (†) superscript will be deleted from concentrations referring to the nucleus. Let us see what Equations (44) and (45) accomplish qualitatively. If, say $\beta_i^{\dagger} \ll \beta_i^0$, with arbitrary γ_i, then

$$\beta_i^* \sim \beta_i^{\dagger} .$$

Hence the slowest mechanism, that of transfer of i across the interface, determines the overall rate. Likewise, for $\beta_i^0 \ll \beta_i^{\dagger}$, and for $|c_i - c_i^0|$ not too small,

$$\beta_i^* \sim \beta_i^0/\gamma_i ,$$

so that the overall rate will be determined by matrix diffusion. Finally, for no partitioning, $\gamma_i \simeq 0$,

$$\beta_i^* \sim \beta_i^{\dagger} ,$$

and only the rate of transfer across the interface influences the effective mobility of i.

Note that nucleation in which matrix and nuclei have same composition can be handled on an ad-hoc basis by this model: in such cases as recrystallization or massive transformations, for which the interface is necessarily incoherent, all γ_i are zero, and the governing rates are those determined by the $\beta_i^{\dagger}$, the interface jump mobilities. Coherent nucleation is handled by essentially setting equal to unity the probability that an atom successfully cross the interface.

The overall effective mobility M* will thus be the one given by Equation (41), with the β_i^*'s replaced by their value from Equation (44). In particular, in the binary case (A-B), we have

$$M^* \sim \frac{\beta_A^*\beta_B^*}{\beta_A^*\cos^2\theta + \beta_B^*\sin^2\theta} , \quad (46)$$

where θ is the angle by which the coordinate system must be rotated so that its axes coincide with the principal directions of W. Equation (46) was originally derived by Reiss (12). In the classical limit of constant-composition embryo growth, we may set (12)

$$\tan \theta = c_B/c_A$$

so that, to a very rough approximation, we have

$$M^* \sim c_A^0 c_B^0 (c_A^2 + c_B^2) \frac{\bar{D}_A \bar{D}_B}{c_A^0 \bar{D}_A c_B^2 + c_B^0 \bar{D}_B c_A^2} \qquad (47)$$

In this equation, we have expressed the effective mobilities, following Equation (42), in terms of effective diffusivities $\bar{D}_i$, which must themselves be evaluated with reference to Equation (44). The hidden temperature dependence of M* is thus to be found in the diffusivities

$$D_i = D_{i,0}\, e^{-Q_i/kT} \qquad (48)$$

in which Q_i is an appropriate activation energy, the preexponential $D_{i,0}$ being only weakly temperature-dependent.

Consider some typical cases:

(1) Dilute solution: the concentration of B in the matrix phase is very low. Then, in this limit,

$$M^* \to \bar{D}_B \, .$$

Furthermore, if $\beta_B^0 \ll \beta_B^\dagger$ (the usual case), M* will be proportional to the intrinsic diffusivity of the minority component B in the matrix phase, as expected.

(2) Concentrated nucleus: the concentration of B in the nucleus is almost unity, whilst that in the matrix is arbitrary. Here again,

$$M^* \to \bar{D}_B \, .$$

This conclusion is valid even if the concentration difference γ is small and/or if the intrinsic diffusivities for matrix diffusion are small; in such cases, the overall rate will be governed by the interface jumping rate of B atoms alone, simply because the nucleus growth process is here purely one of B accretion.

(3) One effective diffusivity much smaller than the other, say $\bar{D}_A \ll \bar{D}_B$, then Equation (47) yields

$$M^* \to \bar{D}_A \, ,$$

i.e., the overall rate will be governed by the slowest moving species, as expected. This latter conclusion is very general and can be derived directly from Equation (41) for an arbitrary n-component system.

(4) Carbon in Iron. Formally, we may regard this case as a binary, the two diffusing species being interstitial C and vacant interstitial sites (V), the Fe toms forming a passive network. Then, as expected, the overall rate will be determined by the effective diffusivity of carbon in the Fe framework. If some slow moving substitutional impurity is added, say Mo, then the quarternary system Fe-Mo-C-V must be considered. The overall rate will be determined by substitutional diffusion in the matrix, and, since Mo is the minority (substitutional) solute in this example, we expect, by Equations (41), (42), (44) and (45),

$$M^* \to \bar{D}_{Mo} \, ,$$

provided that γ_{Mo} is not too small, i.e., that Mo partitioning does occur. In the case of no partitioning, the rate would be governed by interstitial Carbon diffusion.

Finally, let us remind the reader that the derivation of Equation (41) rested on taking the flux vector at the saddle point (J_I^*) to be parallel to the direction of steepest descent from the pass, thereby neglecting the skewing effect of unequal monomer mobilities. This is not quite correct: Actually, the flux vector will rotate away from the W gradient, thus taking the path of traverse to somewhat higher altitudes over the pass, still passing over the point $\underset{\sim}{N}^*$. It can be shown from the positive definite nature of $\underset{\sim}{B}^*$, however, that no matter how different is the mobility matrix from the identity matrix, the flux direction will never rotate outside that portion of the W surface which is located below its tangent plane at $\underset{\sim}{N}^*$, a portion defined by the so-called asymptotic directions (32). Certain proposed prescriptions (16) for estimating the flux direction apparently do not conform to this requirement. Thus, the growing nuclei cannot be denied entrance into the lush valley beyond the pass, but they may be forced by unequal mobilities to take a less than energetically optimal path, with smaller curvature $|\lambda_1|$. Hence, the Zeldovich factor will have to decrease, thereby slowing down the nucleation kinetics. This, however, is a rather small effect compared to the uncertainties in knowledge of the magnitude of W* and of activation energies for diffusion, which uncertainties enter into the problem exponentially. Therefore, getting an incorrect Zeldovich factor appears to be a small price to pay for obtaining an explicit expression for the effective mobility M* in Equation (41).

Various ad-hoc correction terms were inserted into the β_I^*'s, of course, and a cautious reader may begin to wonder what may be the value of this whole exercise. Well, a more thorough analysis of the assumptions of nucleation kinetics show that the range of applicability (classical limit) of the entire theory itself is very narrow indeed, a far more serious criticism. A qualitative discussion of this topic will now be presented.

3.4. Nucleation Far From Equilibrium

It is not our purpose to discuss the validity of the assumptions on which rests classical nucleation theory. Clearly, one does not expect neat little spherical embryos in multicomponent fluids to grow in size in an untransformed, perfectly uniform matrix, their motion over the W surface being fully governed by the Fokker-Planck equation (28). In the classical view, embryos in no way interact with one another, their location in space remaining unspecified. Yet, cluster correlations should certainly be taken into account and some progress has recently been made in this direction: for instance, Binder and Stauffer (16) have included a non-linear "coagulation" term in their kinetic equation, thus allowing for the coalescence of neighboring clusters. As one might expect, however, the mathematics then becomes quite untractable. Also, McGraw and Reiss (33) have shown how the introduction of excluded volume considerations could explain discrepancies observed by Heady and Cahn (34) between measured and observed nucleation rates in a well-characterized binary fluid.

Our aim here is simply to inquire about the general applicability of the classical limit treatment, whereby the nucleation rate can be calculated approximately by saddle point integration, i.e., by assuming the flux J*

to be confined to a very narrow, flat channel whose axis lies in the constant-composition direction in N-space. If these conditions are met, the kinetic method presented above (perhaps with a better diagonalization procedure) may give reliable results. It will appear, however, thatthe classical limit is valid in a very narrow range; beyond that range, an appropriate theory must merge gradually and continuously into a spinodal-type theory. The latter theory, which at first glance appears to be so different in spirit from nucleation theory, will be briefly described in the next section.

The question posed here is not merely of academic interest, as transformations in industrial alloys usually occur far from equilibrium. Since coherent nucleation or precipitation is often associated with transformations at large undercoolings, or high supersaturations (deep quenches), we shall use from the start a coarse-grained free energy function such as the one shown in Figure 5, appropriate for "coherent" transformations. Only binary (fluid) solutions will be considered in this and the next section.

The important features of the required energy curve (Figure 5) can be well represented by the symmetric function

$$f(x) = (x^2 - a_0^2)^2 \tag{49}$$

where f represents an energy per unit volume, x represents a concentration measured away from the central one, and $a_0(P,T)$, the only parameter used, fixes the points of common tangency (at $\pm a_0$). A plot of f(x) for $a_0 = 1$ is shown in Figure 5. Also shown is the tangent at some point $-1 < x_0 \leq 0$. It will be convenient to measure the vertical distance from the tangent at f(x) to the point of tangency, thus

$$\Delta f(\xi) = \frac{1}{4!}f_0'''' \xi^4 + \frac{1}{3!}f_0''' \xi^3 + \frac{1}{2}f_0''\xi^2 , \tag{50}$$

where ξ is the concentration deviation

$$\xi = x - x_0 ,$$

and where the f_0 symbols refer to successive derivatives of f(x) evaluated at the point of tangency. By Equations (49) and (50), Δf can be written

$$\Delta f(\xi) = \xi^2\psi(\xi) \tag{51}$$

with

$$\psi(\xi) = \xi^2 + 4x_0\xi + 2(3x_0^2 - a_0^2). \tag{52}$$

Thus, $\Delta(\xi)$ is none other than the function ΔG_v defined in Section 2.1. By Equation (52), it is seen that the inflection points of $\Delta f(\xi)$ [or of f(x)] occur at

$$x_0/a_0 = \pm 1/\sqrt{3} .$$

Such is the origin of the "root-three rule" (35) for constructing the spinodal curve associated with a given free energy function.

Let us use this function in conjunction with a Rayleigh-Ritz treatment of the Cahn and Hilliard formulation. For that, let us define a standard spherical embryo by the parametrised composition profile (23)

$$c(r) = \xi\, u(\eta,\alpha)$$

where ξ, which appears as an order parameter, is the amplitude of the fluctuation of standard shape $u(\eta,\alpha)$ in which α represents a set of auxiliary parameters defining the shape of the standard profile. Letting $\eta = r/\rho$ allows one to define an effective fluctuation radius ρ, r being the radial distance. For present purposes, it suffices to adopt the capillarity assumption, which consists in regarding the embryo as having constant composition $x_0 + \xi$, separated from the matrix of uniform composition x_0 by a sharp interface at $r = \rho$. Hence, the standard profile may be defined by

$$u(\eta) = \begin{cases} 1 \text{ if } 0 \leq \eta < 1 \\ 0 \text{ if } \eta > 1 . \end{cases}$$

In a sense, then, we have replaced the profile of Figure 3b by that of 3c.

For use in the C-H free energy functional (17), we shall need the integrals

$$4\pi \int_0^\infty [c(r)]^n\, r^2\, dr = \frac{4}{3}\pi\rho^2\xi^n , \tag{53}$$

and

$$4\pi \int_0^\infty \left(\frac{dc}{dr}\right)^2 r^2\, dr = \frac{4}{3}\pi\rho\xi^2 , \tag{54}$$

the latter result having been obtained by noting that the derivative of a function at a discontinuity is the Dirac delta function times the height of the discontinuity. Integral (54) multiplied by the positive gradient energy coefficient κ represents the interfacial energy contribution σA of the classical theory. A similar expression for σ was obtained by Reiss and Shugard (13) who used more elaborate bond counting within the framework of the regular solution model. Through the use of Equation (10), these authors were able to take into account the concentration-dependence of the interface.

In the present formulation, equivalent to that of R-S (13), the work of formation of a standard embryo of amplitude ξ and of radius ρ can be written

$$W = \frac{4}{3}\pi\, [\psi(\xi)\rho^2 + \kappa]\rho\xi^2 \tag{55}$$

with ψ given by Equation (52). As an aid in visualizing this surface, computer-generated contour plots are reproduced in Figures 8a, b, c, d, and e, corresponding respectively to supersaturations $x_0 = -.99, -.95, -.90, -.70, -.10$; values $a_0 = \kappa = 1$ were chosen, and the contours were measured in units of $3/4\pi$. The presence of the ξ^2 factor in Equation (55) produces a zero-level valley (or ridge) all along the ρ axis, whilst the presence of the ρ factor produces zero altitude along the ξ axis, from which the surface gently rises linearly towards larger radii ρ. In all cases, a deep valley is found at large ρ in the vicinity of the ξ value marked $\bar{z}^{(2)}$ in Figure 5. The valley contours are asymptotic to vertical lines at points marked $z_0^{(1)}$ and $z_0^{(2)}$ in Figure 5. Any constant ρ section exhibits a curve made up of $\Delta f(\xi)$ multiplied by ρ^3, representing the bulk free energy, plus a parabola $\kappa\xi^2$ multiplied by ρ, representing the surface free energy. At small ρ, the latter dominates, at large radius, the bulk dominates, as expected.

For all values of x_0 outside the spinodal

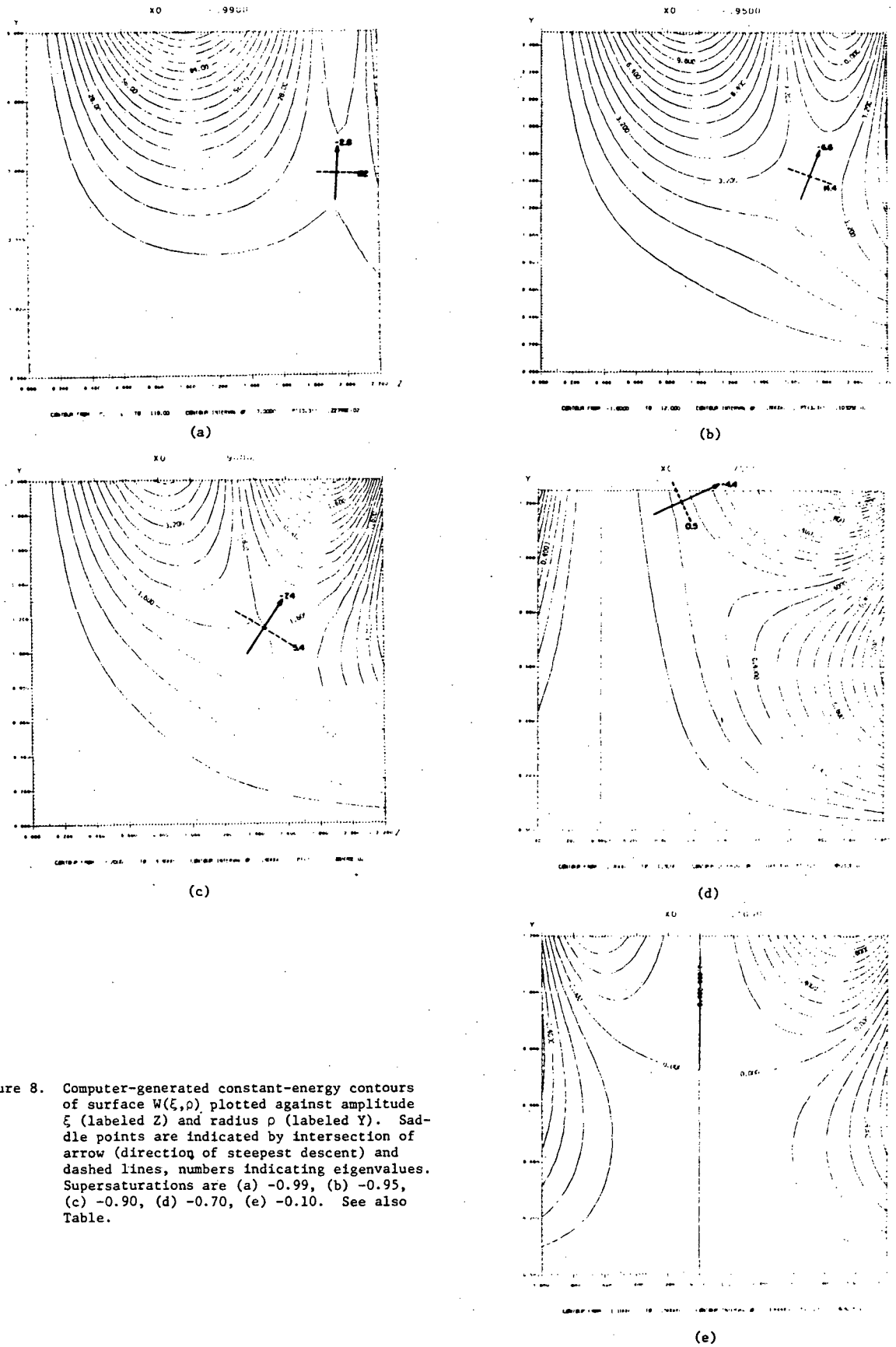

Figure 8. Computer-generated constant-energy contours of surface $W(\xi,\rho)$ plotted against amplitude ξ (labeled Z) and radius ρ (labeled Y). Saddle points are indicated by intersection of arrow (direction of steepest descent) and dashed lines, numbers indicating eigenvalues. Supersaturations are (a) -0.99, (b) -0.95, (c) -0.90, (d) -0.70, (e) -0.10. See also Table.

$$|x_0| > 1/\sqrt{3} ,$$

the W-surface has a saddle point or pass which the growing nuclei must negotiate before they can tumble down into the valley below. The saddle point is indicated in Figures 8a, b, c, and d by the intersection of two line segments, one full which indicates (arrow) the steepest descent from the pass, the other (dashed) which indicates the steepest rise. Numbers alongside these directions are the values of the positive and negative curvatures, respectively.

From Figure 8a, it is apparent that supersaturation $x_0 = -.99$ is within the classical limit: the path over the pass is roughly parallel to the ρ axis (thus at constant composition ξ), the pass very narrow (very large positive eigenvalue), the path level (rather low negative eigenvalue), the altitude very high. Since the flux is concentrated in a narrow, level stream, we may expect that the nucleation flux will be given rather accurately by J* obtained by saddle point integration. The actual trajectories of embryos will be rather complex, however: they start from the region of the origin ($\rho \simeq 0$, $\xi \simeq 0$) as small clusters of small amplitude, and then fan out in all directions of the positive ξ,ρ quadrant. This initial spreading is due to the first term in the Fokker-Planck (F-P) equation (28), which is the Laplacian of $C(\underset{\sim}{N})$, a dissipative term which tends to oppose high local cluster concentrations. As embryos move away from the origin, however, the W-surface relief increases, and soon the influence of the second term of Equation (28) is felt, tending to push the embryos back down the W-surface gradient. During this part of the embryo's journey, the dissipative and drift terms of the F-P equation act in opposition. Eventually, the embryo trajectories will bend upwards and form a dense narrow bundle of flow lines over the pass. Thus, the nature of the pass at low supersaturations is such as to give an integrated flux $\underset{\sim}{J}$* whose orientation will neither depend greatly on the history of the trajectories before the pass, nor on the skewing effect of the mobility matrix $\underset{\sim}{B}$.

At slightly larger supersaturations, the situation is no longer as straightforward. Already, for $x_0 = -.95$ (Figure 8b), i.e., only 2.5% away from the equilibrium concentration ($x^\alpha = -1.0$), measured with respect to the common tangent interval ($x^\beta - x^\alpha = 2.0$), the eigenvectors at the saddle point have rotated away from the coordinate axes directions. The pass is now also much wider, the path not as level. Even with $\underset{\sim}{B}$ close to the identity matrix, the flux direction at the saddle point cannot be determined from a local analysis only: the whole steady-state differential equation should be solved.

Non-classical behaviour is accentuated as the supersaturation increases: for $x_0 = -.90$ (Figure 8c), only 5% away from equilibrium x^α, the eigenvectors at the saddle point have rotated by almost 45° and the negative curvature is now greater than the positive one. Whatever one may say about J* without actually solving the equation, it is clear that nuclei will not cross the pass at constant composition. The pass being low and broad, the flux will be correspondingly diffuse and spread out.

For $x_0 = -.70$ (Figure 8d), still a bit of a way from the spinodal ($x_s = -.577$), all resemblance to classical nucleation has long vanished: those nuclei which cross the pass will do so at almost constant radius, but increasing amplitude, the direction of J* over this very wide flat, low plateau depending significantly on the individual mobilities.

Beyond the spinodal, the W-surface no longer has a saddle point, so that no activation barrier for nucleation exists. For example, at $x_0 = -.10$ (Figure 8e), almost at the symmetric composition, embryos are expected to flow up the radius axis in a very wide stream, spreading out towards both positive and negative amplitudes ξ. Only those embryos whose trajectories remain centered on the ρ axis will encounter no rise in altitude, and therefore no activation energy barrier. However, the dissipative term in the F-P equation will drive a great many embryos away from the ρ axis, forcing them to climb over a low ridge before entering the promised land, the valley beyond. Since both left and right valleys will eventually become populated, the transformation product is expected to consist of large positive and negative-amplitude clusters sharing the available space. A picture of a quasi-periodic modulated structure thus comes to mind, i.e., a typical spinodal structure. Such a conclusion can be arrived at by a completely different argument, as will presently be shown.

Table

x_0	Figure 8	ρ^*	ξ^*	W^*	λ_1^*	λ_2^*
-0.999	not shown	9.15	1.99	24.25	- 0.9	6053.7
-0.99	a	2.95	1.94	7.41	- 2.8	182.0
-0.95	b	1.44	1.71	2.82	- 6.6	14.4
-0.90	c	1.14	1.45	1.59	- 7.4	5.4
-0.70	d	1.21	0.51	0.21	- 4.4	0.5
-0.60	not shown	2.57	0.09	0.01	-10.0	0.007
-0.577	not shown	$\to \infty$	0	0	--	--

To summarize, the above table lists, in order, the critical radius ρ^*, critical amplitude ξ^*, and critical work W^* for increasing values of the supersaturation x_0 at constant temperature. Although the simplest possible Rayleigh-Ritz procedure has been used to minimize the functional ΔF of Equation (17), the essential results of the C-H diffuse interface theory are correctly reproduced, indicating that it is not so much the diffuse nature of the interface which is important, but its composition dependence. It is seenclearly from the table that the critical radius ρ^* starts out to be very large, then decreases as supersaturation increases, only to increase again without limit as the spinodal x_s is approached. Simultaneously, both critical amplitude ξ^* and critical work W^* decrease steadily to zero. However, as explained above, the relief features in the vicinity of the pass become so diffuse at high supersaturations (or low undercoolings) as to make the exact position of the saddle point position and altitude largely irrelevant. Indeed, details of the W-surface relief are ignored by the system when mean altitudes drop below a few kT. Thus, there can be really no "singularity" at the spinodal, and no abrupt change in mechanisms. The spinodal region can in fact be considered as an extension of the nucleation region, albeit non-classical, and conversely. This general conclusion was already drawn from an early study of spinodal decomposition (36, 37), and was reiterated in many other publications (11, 16, 24, 25). The cluster dynamics theory of Binder and co-workers (16) in principle can cover the whole range of supersaturations, but the complexity of the mathematics renders the theory all but inextricable, and comparison with experiment practically impossible.

3.5. Spinodal Decomposition

Spinodal decomposition, discovered theoretically by J. W. Cahn in 1960 (38, 39) has been reviewed a number of times (8, 9, 10). We shall here follow the latter reference, restricting our attention to binary solutions (A-B), with $c(\underset{\sim}{x},t)$ being the only independent composition variable, with $\underset{\sim}{x}$ a position vector in the liquid or solid solution, t the time.

Since neither A or B atoms may be destroyed in unit volume (vacancies not considered), we may write a continuity equation for the concentration $c \equiv c_B$:

$$N_V \frac{\partial c}{\partial t} = - \underset{\sim}{\nabla} \cdot \underset{\sim}{J}$$

where N_v is the number of atoms per unit volume. Note that we are dealing here with actual atomic concentrations, defined by an appropriate coarse-graining, not a cluster concentration as in Equation (27). The net flux $\underset{\sim}{J}$ of B atoms is given by

$$\underset{\sim}{J} = - N_v M \nabla \Phi$$

where M is a suitable positive mobility. The potential Φ will be derived from the C-H free energy functional (12). In the absence of concentration gradient contributions, Equation (15) yields, for the Lagrange multiplier

$$\lambda = f'(c) = \mu_B - \mu_A \ .$$

Since λ appears as a difference of chemical potentials, it may be identified with the potential for atomic diffusion in the usual Fick's law formulation. By analogy, in the present case, let us identify Φ with λ obtained by inserting the Lagrangian (14) into the Euler equation (13). There results

$$\Phi \equiv \lambda = f'(c) - 2\kappa\nabla^2 c \ .$$

The resulting diffusion equation is then

$$\frac{\partial c}{\partial t} = \nabla M \nabla \Phi \ . \qquad (56)$$

This differential equation is non-linear in the unknown concentration $c(\underset{\sim}{x},t)$. A solution in closed form is thus out of the question, although certain basic properties of the solution have been examined by Cahn (38) by a perturbation method. Computer-generated numerical solutions of Equation (56) have provided some insight into the clustering kinetics in binary solutions (36), and these results will be briefly summarized.

When information about the approximate free energy curve is incorporated via $\Phi(c)$ into Equation (56) the solution to the diffusion equation correctly obeys the phase diagram without requiring additional constraints. Examples of such well-disciplined solutions are given in Figures 9a-d, which represent numerical calculations of the evolution of one-dimensional concentration profiles in Al-Zn solid solutions during isothermal aging at 100°C (36). The initial concentration variation $c(\underset{\sim}{x},0)$ was a small-amplitude fluctuation which is not shown in these figures. The thermodynamic parameters used were those calculated by Rundman and Hilliard (40) for the Al-Zn system. The numerical solution $c(\underset{\sim}{x},t)$ of Equation (56) was obtained by a Fourier space forward difference iteration scheme.

Each figure shows concentration profiles as a function of distance for successive aging times. The horizontal full lines indicate the average composition c^0, the dashed lines indicate the (coherent) equilibrium compositions c^α and c^β. The results for a 37.5 at.%Zn alloy (i.e., for c^0 close to the center of the miscibility gap) are shown in Figure 9a: The profiles are quasisinusoidal with bounded amplitude. Further growth of the composition modulation requires a lengthening of the pseudoperiod, which does not take place readily due to the extreme resistance to coarsening of such regular one-dimensional structures.

Figures 9b and c are relative to a 22.5 at.%Zn solution, which is closer to the spinodal composition at 100°C. A striking feature of the profiles is the appearance at an early stage of "Guinier zones" (41) consisting of Zn-rich peaks surrounded by denuded Al-rich regions. This result, which confirms the qualitative arguments put forward by Bonfiglioli and Guinier (42) is a direct consequence of the asymmetric location of c^0 with respect to the miscibility gap boundaries. At this composition, the Guiner zone structure is eventually followed by a well-defined periodic profile which correctly obeys the phase diagram. After prolonged aging the solution displays coarsening effects (Figure 9c), which are apparently less sluggish than those of the symmetric composition (center of the miscibility gap). To quote Hilliard (9), "It is rather remarkable that a single equation can depict the complete life cycle, from birth to death, of a particle."

For compositions still closer to the spinodal (Figure 9d; 20 at.%Zn), an early-stage coarsening reaction sets in and the secondary maxima of the Guinier zones dissolve before they have a chance to develop into full-fledged precipitates as they did in the previous case. Thus a periodic structure fails to develop for this asymmetric composition although the average composition is still within the spinodal. Actually, the final concentration profile peaks at the spots where the first maxima make their appearance; in other words, the location of the precipitates is dictated almost entirely by the vagaries of the initial fluctuation, a characteristic more reminiscent of nucleation than of "typical" spinodal decomposition.

Subsequently, the elegant theory of Langer et al. (24, 43) confirmed and expanded these results which were initially confined to one-dimensional concentration profiles. Here also, we see that the spinodal in no way separates clustering kinetics into two competing irreconcilable mechanisms. Rather, at one extreme, the classical nucleation limit, nucleation theory gives a satisfactory account of the transformation, where cluster formation kinetics is of paramount importance and cluster correlations less so. At the other extreme, deep inside the spinodal, at close to maximum supersaturation (or deep quench), cluster kinetics are less important than spatial correlations, and classical spinodal theory works best. Unfortunately, as mentioned previously, no single tractable theory exists for the whole range of supersaturations. This point is also made quite clearly in Martin's excellent review article on the subject (11).

For the practical physical metallurgist, neither Fokker-Planck equations nor non-linear spinodal equations are of much use, however. In practice, then, there is little else to be done but to trust the limiting-case theories: saddle point integration at one extreme and linear spinodal theory at the other, with nothing but a prayer in between. With these words of caution, let us now briefly describe the linear spinodal theory as Cahn originally developed it (38).

For average compositions and aging temperatures well inside the spinodal and, in particular, for c^0 in the vicinity of the center of the miscibility gap, the absolute value of the ratio of the third to the second derivative of f(c) is small compared to unity, and the second-degree term in c can be initially neglected in the potential $\Phi(c)$. The third-degree term in the potential can also be neglected initially, since its magnitude is proportional to the third power of the composition variation, a small quantity. It follows that under the above conditions, the potential function $\Phi(c)$ can be linearized, and this leads to the following diffusion equation (38)

$$\frac{\partial c}{\partial t} = M(f_0'' \nabla^2 c - 2\kappa\nabla^4 c) \ , \qquad (57)$$

where M and κ are assumed to be concentration and time independent, and where f_0'' represents the second derivative of the "incoherent" free energy evaluated at $c = c^0$. Equation (57) can be Fourier-transformed to an ordinary differential equation whose solution is found to be

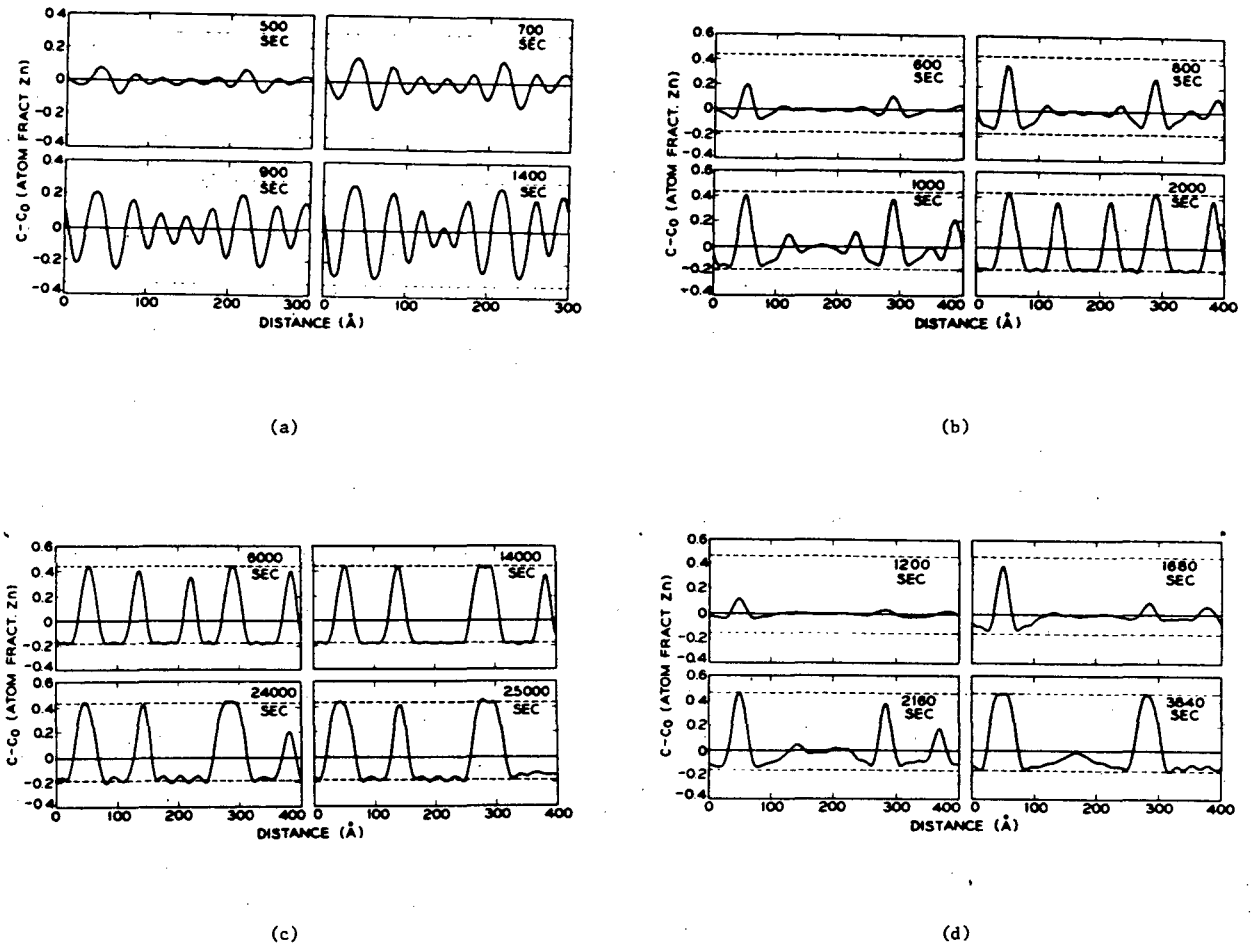

Figure 9. Concentration profiles calculated (36) according to one-dimensional non-linear diffusion equation (56) for an Al-Zn alloy aged at 100°C for the indicated durations and for concentrations: (a) 37.5 at.%Zn, (b) 22.5 at.%Zn, (c) same as (b), longer times, (d) 20.0 at.%Zn.

$$X(\underset{\sim}{k},t) = X(\underset{\sim}{k},0)\, e^{\alpha(\underset{\sim}{k})t} \qquad (58)$$

with amplification rate

$$\alpha(\underset{\sim}{k}) = -Mk^2(f_0'' + 2\kappa k^2) \; . \qquad (59)$$

In these equations k^2 is the square of the wave vector $\underset{\sim}{k}$ and X is the Fourier transform of the concentration deviation ξ, $X(\underset{\sim}{k},0)$ being the Fourier transform of the initial concentration fluctuation.

Equation (59) shows that the Fourier amplitudes of concentration waves initially grow ($\alpha > 0$) or decay ($\alpha < 0$) in time according to an exponential law. Two important quantities were introduced by Cahn (38): the critical wave number k_c, solution of

$$\alpha(k) = 0 \; ,$$

and the optimum wave number k_m, solution of

$$\frac{d\alpha}{dk} = 0$$

for a particular direction $\underset{\sim}{k}$.

The physical meaning of these concepts is best discussed in terms of wavelengths Λ, inversely related to wave number by

$$\Lambda = 2\pi/k \; .$$

Within the framework of the linear theory, all harmonic composition waves of wavelength Λ larger than the critical wavelength

$$\Lambda_c = 2\pi \sqrt{-2\kappa/f_0''} \qquad (60)$$

will grow in amplitude as isothermal aging progresses, while those with $\Lambda < \Lambda_c$ will decay. Maximum growth in a given direction $\underset{\sim}{k}$ will occur for the optimum wavelength

$$\Lambda_m = \Lambda_c\sqrt{2} \ . \qquad (61)$$

These considerations are valid only for the initial stages of spinodal decomposition, well inside the coherent spinodal. Outside the spinodal, the linear approximation breaks down completely since, by Equation (59), Λ_c and therefore also Λ_m are imaginary quantities. This is because, since κ is positive for a clustering system, the quantity under the radical in Equation (60) can only be positive for $f_0'' < 0$, which defines the region inside the spinodal.

In a further development of the theory, Cahn (39) introduced an important correction term to f_0'' to take into account anisotropic elastic coherency strains which must develop during growth of concentration waves in crystalline solids. This topic will not be covered here, however.

Spinodal theory has received ample experimental justification, as periodic, or pseudo-periodic microstructures have been reported in binary liquids, in binary and ternary alloys, and in minerals [see, for example, the articles by Hilliard (9), Martin (11), Grilhé (44) for pertinent bibliography]. In more recent experimental work (45, 46, 47) the trend is to analyze the data, particularly the structure factor obtained by small angle X-ray or neutron diffraction, in terms of scaling laws (48).

3.6. Homogeneous/Heterogeneous Nucleation

Elaborate models of unmixing (clustering, phase separation) may be of considerable theoretical interest, but are of little use to the physical metallurgist interested in understanding microstructure resulting from various heat treatments of alloys. Ideally, one would like to put theoretical models to good use by predicting, say, annealing times and temperatures required to produce specified microstructures. In that context, pushing a simple theoretical model beyond its domain of applicability may result in a numerical error of a factor of two or three perhaps, whereas the use of slightly incorrect values of some of the parameters may lead to results which are off by several orders of magnitude.

It is apparent that, if we adopt J* given by Equation (37) as a measure of the nucleation rate, a small change in the value of W*, especially at temperatures not too high, will have drastic consequences. In particular, by Equation (11) for W*, we see that a slight change in the value of the interfacial energy σ, or of the driving force ΔG_V^* will have profound repercussions on J*, these changes occurring as they do in the parameters raised respectively to the third and second power of the arguments of an exponential function! Small wonder that very little quantitative agreement is usually encountered between experiment and nucleation theory. This is particularly true for nucleation in solids, as effects of strain energy, anisotropic interfacial energy, preferential nucleation sites and other factors play a decisive role in the kinetics.

It would take us too far afield to cover these topics; the interested reader is referred to K. C. Russell's excellent recent review of nucleation in solids (5), which it would be pointless to attempt to duplicate. A very thorough and complete but older treatment is also to be found in J. W. Christian's classic treatise (2). Here, let us merely point out the essential features which must be considered when discussing nucleation in solids.

First of all, a distinction must be made between homogeneous and heterogeneous nucleation, that is to say, between nucleation initiating at arbitrary sites in the bulk, essentially perfect crystalline phase, and that initiating at preferential nucleation sites such as grain or phase boundaries or other imperfections. A further distinction must also be made between nuclei growing coherently and those growing incoherently in the matrix. By the word coherent we mean that, strictly, the matrix and the nucleus have same crystalline lattice, with perhaps a small change in lattice parameters; in other words, there is perfect coherence if the lattice planes suffer no discontinuities at the matrix-nucleus interface. On the contrary, by the word incoherent is meant that there is no matching of crystalline directions or lattice spacings on either side of the interface. Intermediate cases are of course often encountered; the word semi-coherent is then used rather indiscriminately either to denote cases in which the mismatch between matrix and nucleus can be accommodated by, say, periodic arrays of interfacial dislocations, or cases where some portions of the matrix-nucleus are coherently related whilst other portions are not.

These morphological distinctions are important as they lead to different values of the effective interfacial energy σ and the driving force ΔG_V. Generally speaking, phase β and phase α will have different molar volumes. In solids, homogeneous coherent nucleation of β from α will thus give rise to strain fields which can be very large and which must add a positive contribution to the negative ΔG_V. Hence, such strain energy contributions, which are evaluated in practice according to linear isotropic elasticity theory, will substantially increase the work of nucleation W* by decreasing the value of the denominator $(\Delta G_V + \Delta G_E)^2$, ΔG_E being the elastic energy contribution. It follows that coherent homogeneous nucleation will require larger undercoolings in order to proceed at appreciable rate.

Coherency strains in homogeneous nucleation can be at least partially relieved by introducing interfacial dislocations whose role is to take up most of the lattice mismatch between α and β. In a sense then, the decrease in magnitude of the driving force due to bulk elastic energy has been replaced by an increase in the interfacial energy σ. Such a substitution can be energetically favorable for nuclei of large radius which have relatively small surface-to-volume ratio. Hence all other things being equal, one may expect coherent nucleation at large supersaturations or undercoolings and incoherent nucleation at lower ones, with, possibly, semi-coherent nucleation in between.

These concepts may be understood with the help of Figure 10 which shows, in the upper portion, schematic plots of free energy curves vs. composition for a binary solid solution. Curves for semi-coherent and coherent B-rich β are shown to lie above that for incoherent β because of the positive elastic contribution ΔG_E to the (negative) total driving force. The curve for coherent β has actually been drawn as the continuation of the α free energy curve since coherent β must be structurally no different from α. By invoking the tangent construction described in Section 2.1, it is expected that, at the temperature (T') considered, incoherent (I) β can nucleate for matrix compositions c^0 located to the right of the common tangency point c_I^α, semi-coherent (S) β can nucleate for compositions c^0 to the right of c_S^α, and coherent (C) β can nucleate for c^0 to the right of c_C^α. At given undercooling or supersaturation, which mode of transformation will dominate depends upon the relative magnitudes of interfacial and bulk energies. For example coherent nucleation will win if its TTT start curve lies at lower transformation times in the temperature range considered than either the semi-coherent or incoherent C-curves.

In Figure 10, separate free energy curves were sketched for the various transformation products envisaged. Hence, by the common tangent rule, three different temperature-concentration phase diagrams could be constructed, as shown at the lower portion of Figure 10. A continuous miscibility gap (C) has been constructed as locus of common tangency points for the continuous (C) free energy curve, whilst only portions of coexistence curves have been constructed for the other two cases, since it cannot be decided without further information what possible three-phase reactions may occur

at higher temperatures: eutectic, peritectic, eutectoid ... . The coherent spinodal, locus of inflection points of the continuous free energy curve, has also been indicated on the phase diagram. Sometimes the following designation is used: phase diagram curve C is called the coherent solvus, curve S the semi-coherent solvus, and curve I the equilibrium phase boundary (if it is indeed the topmost one). Sometimes also, these curves may be labeled according to the conventional symbol attached to the nucleating phase: GP zone, θ", θ' ... in the case of Al-Cu alloys, for example. To illustrate the use of the phase diagram in the present context, consider a homogeneous solid solution of average composition $c^0 = c^{\alpha}_S$, say. Then, coherent nucleation can only take place at temperatures below T_C (Figure 10), semi-coherent below T' (≡ T_S), and incoherent below T_I.

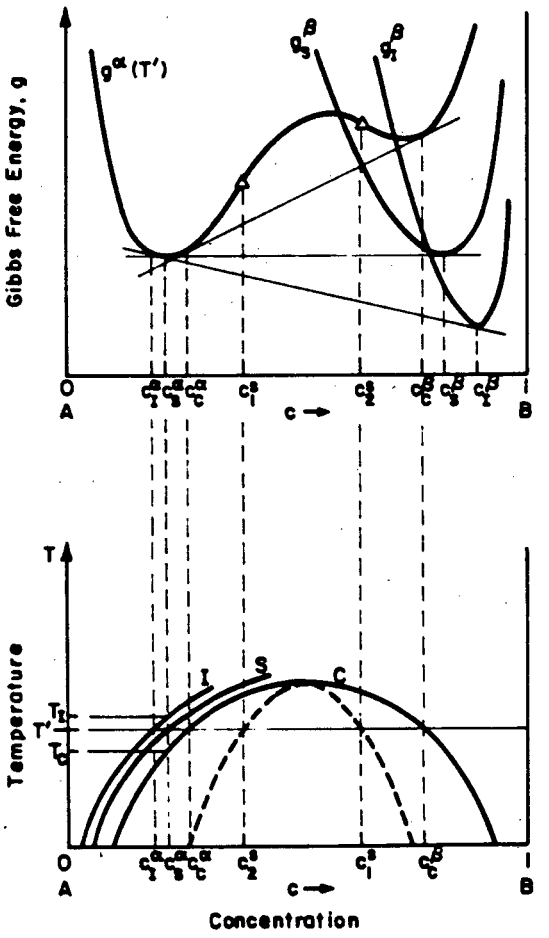

Figure 10. Free energy curves (top) for binary alloy and associated phase diagram (bottom) for incoherent (I), semi-coherent (S) and coherent (C) phases.

Without interfacial energy, there would be no activation barrier for nucleation. Although the positive contribution of σ cannot be eliminated, it can be reduced in so-called heterogeneous nucleation, as opposed to homogeneous nucleation considered up to now. It is well documented that imperfections are able to catalyze the nucleation process: in essence, the nucleus, by attaching itself to a preexisting high-energy surface (grain boundary, interphase boundary, free surface, etc.), replaces a portion of existing matrix-defect boundary by an identical portion of nucleus-defect boundary plus a matrix-nucleus portion. In many cases (depending on the relative magnitudes of the interfacial energies involved) this can be energetically far more favorable than the creation from scratch of a complete matrix-nucleus boundary of approximately same total area. In typical cases, one can calculate effective reduced interfacial energies (σ_{eff}) to be inserted in the critical work formula (11) for W*. As σ comes with third power into the exponential for the nucleation rate, even a small reduction in effective interfacial energy can enhance nucleation rates by many orders of magnitude. At low undercoolings, then, we expect heterogeneous nucleation to be kinetically favored whilst at large undercoolings homogeneous nucleation may prevail. The reason is that the larger σ which accompanies homogeneous nucleation may be offset partially by the larger driving force $|\Delta G_v|$ available and that, importantly, coherent nucleation will have much larger prefactor K in the rate expression (37) for J*, simply because so many more sites for homogeneous nucleation are available over those available for various types of heterogeneous nucleation. In this context, Cahn (49) has given an interesting discussion of site availability and saturation.

4. TTT DIAGRAMS

We may now return to the topic with which we opened this paper: that of TTT diagrams. Let us first see whether nucleation theory and its ramifications help to understand the simple C-curve diagram, such as that of Figure 1, for a plain carbon eutectoid steel.

4.1. C-Curves

Let us make the simplest possible assumptions: although the position of the start curve should be obtained by calculating the incubation time for copious nucleation, we shall, for simplicity, regard the start time t_S as the reciprocal of the steady-state nucleation rate as calculated by saddle-point integration. Furthermore, we shall assume that a single temperature-independent activation energy for diffusion Q dominates the effective mobility M* [see discussion accompanying Equations (41) and (44), especially case (4)]. Then we have

$$\text{Rate} \simeq J^* = K_0 \, e^{-(W^* + Q)/kT}$$

where K_0 contains all factors not included in the exponentials. The start time t_S may thus be given by

$$\log t_S = - \log K_0 + \Gamma(T) \qquad (62)$$

with

$$\Gamma(T) = m(W^* + Q)/kT \qquad (63)$$

and

$$m = \log e = 0.4343...$$

Although, in the present case, pearlite (α iron + carbide) most certainly does not nucleate in bulk γ Austenite as small spherical homogeneous embryos, we shall nevertheless use Equation (11) for estimating the temperature dependence of W*.. In this equation, the volume energy (driving force) may be written

$$\Delta G_v = \Delta H_v - T\Delta S_v ,$$

where ΔH_v denotes the enthalpy difference and ΔS_v the entropy difference per unit volume between the nucleating phase and the tangent to the parent phase at same composition, temperature and pressure. At the equilibrium temperature T_0 (common tangent rule) we must have

$$\Delta G_v = \Delta H_v - T_0\Delta S_v = 0 ,$$

If the enthalpy and entropy differences are assumed to vary but little with temperature, we find

$$\Delta H_v = T_0\Delta S_v$$

and hence

$$\Delta G_v = (T - T_0)\Delta S_v .$$

The strongly temperature-dependent part of log t_S may thus be written, by Equation (63), as

$$\Gamma(\tau) = m\,\frac{16\pi\sigma^3}{3kT_0\Delta H_v^2}\left[\frac{b}{\tau} + \frac{1}{\tau(1-\tau)^2}\right] \qquad (64)$$

where

$$\tau = T/T_0$$

is a reduced temperature and

$$b = \frac{3Q\Delta H_v^2}{16\pi\sigma^3} \qquad (65)$$

is a dimensionless parameter which, in this approximation, completely determines the shape of the start curve. We shall assume for simplicity that the coefficient of the bracketed term in Equation (64) is roughly temperature-independent. Then, knowledge of the "nose" temperature τ_N fixes the value of this parameter

$$b = \frac{3\tau_N - 1}{(\tau_N - 1)^3} . \qquad (66)$$

Since the nose of the experimental curve of Figure 1 is located at about $T_N = 0.825\ T_0$, we shall take $b \simeq 275$, according to Equation (66). The resulting start curve is shown in Figure 11. The simplifications used in its derivation were so drastic that quantitative agreement is hardly to be expected. Nevertheless, the calculated curve of Figure 11 does reproduce the essential features of a typical C-curve (Figure 1), the most obvious discrepancy being the calculated curve's reluctance to reach its asymptote T_0 at reasonable times t. When realistic physical parameters are inserted into Equation (65), it is found that a value of $\sigma \simeq 60$ ergs/cm^2 must be chosen in order to obtain the selected value for b. Such a low value does not seem out of line for an effective interfacial energy for heterogeneous nucleation, however.

4.2. S-Curves

It is reasonable to interpret an S-curve (Figure 2) as the combination of two C-curves. This idea is illustrated schematically in Figure 12. The two distinct transformations which each yield their separate C-curves require separate nucleation events, one associated with the equilibrium transition temperature T_0, taken in Figure 12 to be that for incoherent equilibrium T_I, and one associated with some lower metastable transition temperature T_C, taken here to be that for coherent (metastable) equilibrium. In the present case, T_I and T_C are thus the temperatures denoted by the same symbols in Figure 10, for example. Of course, the lower C-curve is not necessarily due to coherent nucleation, but at least we know from our lengthy analysis of nucleation far from equilibrium that it cannot be due to spinodal decomposition.

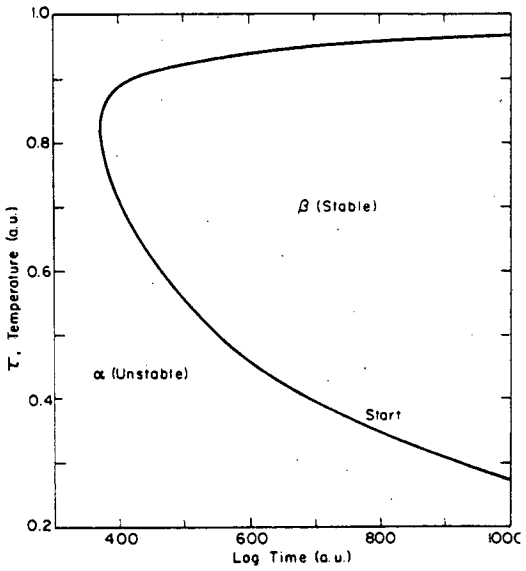

Figure 11. C-curve calculated according to equation (64) with b = 275. Compare with Figure 1.

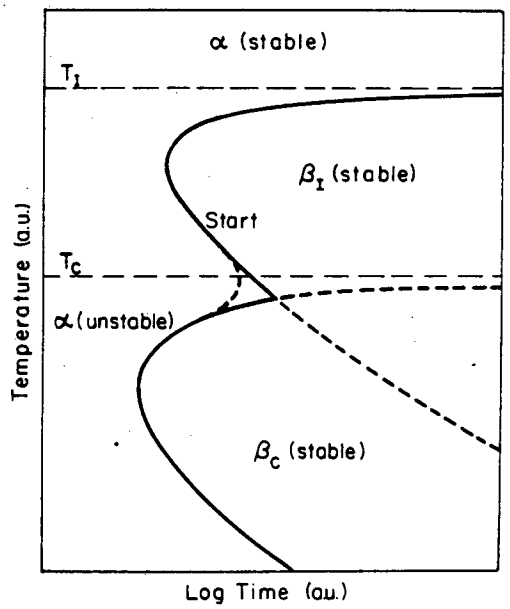

Figure 12. Schematic construction for S-curve. T_I and T_C are temperatures for incoherent and coherent transformations, respectively.

The situation in alloy steels is more complicated (see example in Figure 2), as the lower portion of the S-curve is surely not due to coherent precipitation but to the appearance of complex carbides which are, at best, semi-coherent with the parent phase. It may at first appear surprising that such minute amounts of a third and fourth constituent (0.45% Mn, 1.97% Cr) should alter so drastically the TTT diagram of steel. It must be recalled from the discussion on mobility (Section 3.3) however, that the temperature dependence of the prefactor K in Equation (37) is governed by the effective mobility M* whose magnitude, in turn, is determined by slowest-moving partitioning solute, even though [case (1)] its concentration in the matrix may be very low. In the present case, both Mn and Cr enter Austenite substitutionally, so that their diffusion rates are much smaller than that of interstitial Carbon. Thus, in accordance with the discussion of case (4), a lateral shift of start times from seconds, in the case of plain Carbon steels, to minutes, in the case of alloy steels, is expected.

But then, what is one to make of propensity of alloy steels to exhibit serpentine TTT diagrams? One may conjecture that in ternary and quaternary systems, the tangent plane at the matrix composition c_i^0 will, at large undercooling, intersect a variety of other free energy surfaces, or portions of free energy surfaces, not normally accessible close to equilibrium. The chosen transformation may then be the one that nucleates metastable products (complex carbides) which require a lesser degree of solute partitioning and which can therefore form more rapidly given an adequate undercooling. The postulated metastable carbides will require for their formation separate nucleation events, and hence separate C-curves. Perhaps the reader will now forgive the author for having treated nucleation theory in its multicomponent form, right from the start: TTT diagrams of complex alloys cannot be understood, even qualitatively, without some grasp of multicomponent theory.

4.3. End Curves

There is one last feature of TTT diagrams which will now be discussed briefly: the "end" curves. These curves are similar to the corresponding start curves but, of course, displaced towards longer times. To obtain some measure of the time required for completion of the transformation, one must inquire into the evolution of embryos after they have overcome the activation energy barrier and grow to full maturity. Clearly, interference between growing nuclei must now be taken into account, as the available volume for nucleation and growth steadily decreases as the transformation progresses.

To handle this "impingement" problem, Johnson and Mehl (50) and Avrami (51) proposed a clever model: these authors introduced the concept of "extended volume" which is the total volume that the growing phase would have occupied (at time t) had it been allowed to grow unimpeded by other transforming regions, and assuming that nucleation would take place anywhere within the sample, including the previously transformed regions. Let V_x denote the entended volume fraction. It is related to the true volume fraction V by the equation

$$dV = (1 - V)\, dV_x ,$$

where $(1 - V)$ is the probability of overlap of a newly transformed region onto a previously transformed one. The integrated form of this equation is

$$V = 1 - e^{-V_x} . \qquad (67)$$

The reason for the introduction of this fictitious volume fraction V_x is that its growth law can be determined in a straightforward manner, whereas that of V cannot. If G(t) is the growth rate of any linear dimension of the new phase, then for isotropic (spherical) growth one obtains the following equation for the extended volume at time t:

$$V_x(t) = \frac{4}{3} \int_0^t I(t) G^3(t') (t - t')^3 \, dt' , \qquad (68)$$

where I(t) now designates the nucleation rate, which could be that given by Equation (37), but will, in general, be time dependent. Equation (68), when introduced into Equation (67), yields the required growth law. Under very general assumptions the resulting growth law will be of the form

$$V(t) = 1 - e^{-At^n} , \qquad (69)$$

where A is an appropriate constant, and where $3 \leq n \leq 4$ for three-dimensional nucleation and growth. A table of values of n for a wide variety of situations is given in Christian's treatise (2). Equation (69) plots as a sigmoid curve exhibiting incubation, growth, and saturation stages. In clustering reactions, saturation sets in with the exhaustion of the supply of available solute atoms and occurs when the volume fraction V has reached its maximum value dictated by the lever rule. The sigmoid curve representing Equation (69) can be roughly approximated by its tangent at the inflection point, and its intercepts at horizontal lines representing, say, 1% and 99% volume fraction transformed, can be taken as measures of the start (t_S) and end times (t_E) respectively. The difference $(t_E - t_S)$ then fixes the position of the end curve, in principle, once that of the start curve is known.

5. EPILOGUE

We have come full circle: what started out, and ended, as a benign description of TTT diagrams, evolved into rather complex theoretical discussions. It should be obvious that enormous gaps separate theory from practical applications. Theorists claim that the theories are either too crude or too difficult to handle, experimentalists claim that the parameters required cannot be obtained with sufficient accuracy, and practical Physical Metallurgists claim (correctly) that no existing model can really do justice to the tremendous complexity of real systems. It is sometimes stated that the gaps are narrowing, but this author is not brimming with optimism: all that he can hope for is that this article will not contribute to the widening of the gaps.

References

1. E. C. Bain and H. W. Paxton Alloying Elements in Steel , ASM, Metals Park, Ohio, 1961.

2. J. W. Christian, The Theory of Phase Transformations in Metals and Alloys, Pergamon, London, 1965.

3. D. Turnbull, "Phase Changes", p. 226-308 in Solid State Physics, F. Seitz and D. Turnbull, eds.; Academic, New York, 1956.

4. K. C. Russell, "Nucleation in Solids", p. 219-268 in Phase Transformations, H. I. Aaronson, ed.; American Society for Metals, Metals Park, Ohio, 1970.

5. K. C. Russell "Nucleation in Solids: The Induction and Steady State Effects", Advances in Colloid and Interface Science, 13 (1980), p. 205-318.

6. H. I. Aaronson, "The Kinetic Equations of Solid-Solid Nucleation Theory", p. 83-115 in Lectures on the Theory of Phase Transformations, H. I. Aaronson, ed.; Met. Soc. of AIME, New York, 1975.

7. J. W. Cahn, "Unmixing in Binary Critical Systems", p. 41-64 in Critical Phenomena in Alloys, Magnets and Superconductors, R. E. Mills, E. Ascher and R. I. Jaffee, eds.; McGraw-Hill, New York, 1971.

8. J. W. Cahn, "Spinodal decomposition", Trans. AIME, 242 (1968), p. 166-180.

9. J. E. Hilliard, "Spindoal decomposition", p. 497-560 in Phase Transformations, H. I. Aaronson, ed.; American Society for Metals, Metals Park, Ohio, 1970.

10. D. de Fontaine, "Clustering Effects in Solid Solutions", p. 129-178 in Treatise on Solid State Chemistry, Vol. 5, Phase Changes, N. B. Hannay, ed.; Plenum Press, New York, 1975.

11. G. Martin, "The Theories of Unmixing Kinetics of Solid Solutions", p. 337-406 in Solid State Phase Transformations in Metals and Alloys; Aussois 1978; Les Editions de Physique, Orsay, France, 1980.

12. H. Reiss, "The Kinetics of Phase Transitions in Binary Systems", Journal of Chemical Physics, 18 (1950), p. 840-848.

13. H. Reiss and M. Shugard, "On the Composition of Nuclei in Binary Systems", Journal of Chemical Physics, 65 (1976), p. 5280-5293

14. J. S. Langer, "Statistical Theory of the Decay of Metastable States", Annals of Physics, 54 (1969), p. 258-275.

15. J. S. Langer and L. A. Turski, "Hydrodynamic Model of the Condensation of a Vapor near its Critical Point", Physical Review A, 8 (1973), p. 3230-3243.

16. K. Binder and D. Stauffer, "Statistical Theory of Nucleation, Condensation and Coagulation", Advances in Physics, 25 (1976), p. 343-396.

17. P. Mirold and K. Binder, "Theory for the Initial Stages of Grain Growth and Unmixing Kinetics of Binary Alloys", Acta Metallurgica, 25 (1977), p. 1435-1444.

18. J. W. Gibbs, "On the Equilibrium of Heterogeneous Substances", p. 55-353 in The Scientific Paper of J. Williard Gibbs, Vol. 1 Thermodynamics, Dover Publ., New York, 1961.

19. E. M. Lifshitz and L. P. Pitaevskii, "Statistical Physics, 3rd Edition, Part 1", p. 536 in Course of Theoretical Physics, Vol. 5, Landau and Lifshitz, Pergamon, Oxford, 1980.

20. J. S. Langer, "Metastable States", Physica, 73 (1974), p. 61-72.

21. J. W. Cahn and J. E. Hilliard, "Free Energy of a Nonuniform System, I. Interfacial Free Energy", J. Chem. Phys., 28 (1958), p. 258-267.

22. J. W. Cahn and J. E. Hilliard, "Free Energy of a Nonuniform System, II. Nucleation in a Two-Compartment Incompressible Fluid", J. Chem. Phys., 31 (1959), p. 688-699.

23. D. de Fontaine, "On the Stability of Spherically Symmetric Compositional Inhomogeneities in Solid Solutions", Trans. Met. Soc. AIME (1969), p. 1703-1709.

24. J. S. Langer, M. Bar-On, and H. D. Miller, "A New Computational Method in the Theory of Spinodal Decomposition", Physical Review A, 11 (1975), p. 1417-1429.

25. K. Binder, M. H. Kalos, J. L. Lebowitz and J. Marro, "Computer Experiments on Phase Separation in Binary Alloys", Advances in Colloid and Interface Science, 10 (1979), p. 173-214.

26. L. Farkas, Zeitsckrift für Physikalische Chemie, 125 (1927), p. 236.

27. M. Volmer and A. Weber, "Nuclei Formation in Supersaturated States", Z. Physik. Chem., 119 (1925), p. 277-301.

28. R. Becker and W. Döring, "Kinetic Treatment of Grain Formation in Supersaturated Vapors", Ann. Physik., 24 (1935), p. 719-752.

29. K. C. Russell, "Linked Flux Analysis of Nucleation in Condensed Phases", Acta Metallurgica, 16 (1968), p. 761-769.

30. J. Frenkel, Kinetic Theory of Liquids, Oxford, University Press, 1946.

31. H. Reiss, "The Number of Unilateral Solute Impacts on Unit Surface in a Dilute Solution", Journal of Chemical Physics, 18 (1950), p. 996-997.

32. D. de Fontaine, "An Analysis of Clustering and Ordering in Multicomponent Solid Solutions—II. Fluctuations and Kinetics", J. Phys. Chem. Solids, 34 (1973), p. 1285-1304.

33. R. McGraw and H. Reiss, "Nucleation Near a Critical Temperature", Journal of Statistical Physics, 20 (1979), p. 385-413.

34. R. B. Heady and J. W. Cahn, "Experimental Test of Classical Nucleation Theory in a Liquid-Liquid Miscibility Gap System", Journal of Chemical Physics, 58 (1973), p. 896-910.

35. H. E. Cook and J. E. Hilliard, "A Simple Method of Estimating the Chemical Spinodal", Trans. Met. Soc. AIME, 233 (1965), p. 142-146.

36. D. de Fontaine, "A Computer Simulation of the Evolution of Coherent Composition Variations in Solid Solutions", Ph.D. Dissertation, Northwestern University, Evanston, Illinois, 1967.

37. D. de Fontaine, "Development of Fine Coherent Precipitate Morphologies by the Spinodal Mechanisms" p. 93-131 in Ultrafine Grain Metals, Burke and V. Weiss, eds.; Syracuse Univ. Press, 1970.

38. J. W. Cahn, "On Spinodal Decomposition", Acta Met., 9 (1961), p. 795-801.

39. J. W. Cahn, "On Spinodal Decomposition in Cubic Crystals", Acta Met., 10 (1962), p. 179-183.

40. K. B. Rundman and J. E. Hilliard, "Early Stages of Spinodal Decomposition in an Aluminum-Zinc Alloy", Acta Met., 15 (1967), p. 1025-1033.

41. A. Guinier, "Nouvelle Interpretation Des Diagrammes à "Side-Bands", Acta Met., 3 (1955), p. 510-522.

42. A. Bonfiglioli and A. Guinier, "La Structure des Zones G. P. dans les Alliages Aluminium-Zinc au Premier Stade de leur Formation", Acta Met., 14 (1966), p. 1213-1224.

43. J. S. Langer, "Statistical Methods in the Theory of Spinodal Decomposition", Acta Met., 21 (1973), p. 1649-1659.

44. J. Grilhé, "Experimental Studies of Decomposition

of a Solid Solution", p. 407-427 in Solid State Phase Transformations in Metals and Alloys; Aussois 1978; Les Editions de Physique, Orsay, France, 1980.

45. N. C. Wong and C. M. Knobler, "Spinodal Decomposition in Isobutyric Acid + Water Mixtures", Journal of Chemical Physics, 66 (1977), p. 4707-4709.

46. G. Laslaz, P. Guyot and G. Kostorz, Journal de Physique C7, 38 (1977); M. Hennion, D. Ronzaud and P. Guyot, "Kinetics of Unmixing in Al-Zn Single Crystals Studied by Neutron Small-Angle Scattering", Preprint, Institut National Polytechnique de Grenoble, LTPCM, ENSEEG Domaine Universitaire, BP 44, 38401 St. Martin d'Hères, France, 1981.

47. Private communication, A. R. Forouhi and J. M. Sanchez, Dept. of Materials Science and Mineral Eng., University of California, Berkeley, 1981.

48. J. Marro, J. L. Lebowitz and M. H. Kalos, "Computer Simulation of the Time Evolution of a Quenched Model Alloy in the Nucleation Region", Physical Review Letters, 43 (1979), p. 282-285.

49. J. W. Cahn, "The Kinetics of Grain Boundary Nucleated Regions", Acta Met., 4 (1956), p. 449-459; Acta Met., 5 (1957), p. 168-175.

50. W. A. Johnson and R. F. Mehl, "Reaction Kinetics in Processes of Nucleation and Growth", Trans. AIME, 135 (1939), p. 416-458.

51. M. Avrami, "Kinetics of Phase Change—I. General Theory", J. Chem. Phys., 7 (1939), p. 1103-1112.

This work was supported by the Director, Office of Energy Research, Office of Basic Energy Sciences, Materials Sciences Division of the U.S. Department of Energy under Contract Number W-7405-ENG-48.

Programming assistance from Dr. W. Teitler is gratefully acknowledged.

This report was done with support from the Department of Energy. Any conclusions or opinions expressed in this report represent solely those of the author(s) and not necessarily those of The Regents of the University of California, the Lawrence Berkeley Laboratory or the Department of Energy.

Reference to a company or product name does not imply approval or recommendation of the product by the University of California or the U.S. Department of Energy to the exclusion of others that may be suitable.

TECHNICAL INFORMATION DEPARTMENT
LAWRENCE BERKELEY LABORATORY
UNIVERSITY OF CALIFORNIA
BERKELEY, CALIFORNIA 94720